People's Democratic Republic of Algeria
Ministry of Higher Education and Scientific Research

University M'Hamed BOUGARA – Boumerdès

Institute of Electrical and Electronic Engineering
Department of Control and Power Engineering

Project Report Presented in Partial Fulfilment of

the Requirements of the Degree of

'MASTER'

In Power Engineering

Title:

Load Flow analysis for Islanded Microgrid

Presented By:

- **BELKADI Yacine**

Supervisor:

- **Pr. Aissa KHELDOUN**

Registration number: ……./2022

Abstract

Due to the increasing demand for green energy these last years, renewable energy sources have been integrated more efficiently with the utility grid. The combination of energy sources, storage devices and the power electronics interface with the aim of satisfying the load is called a microgrid. A microgrid can deliver energy autonomously in the islanded mode, which make the object of electrifying the remote areas purely using renewable energy doable. The conventional load flow techniques cannot be implemented on the islanded microgrid because the voltage of slack bus and the frequency are assumed to be constant. This assumption fails to consider the real characteristics of the islanded microgrid where all the distributed generators share the load demand and the losses as well as maintaining the frequency.

In this project, the conventional load flow technique using Newton Raphson is modified, combined with the droop control concept to predict efficiently the behaviour of an islanded microgrid. This prediction allows to compute the active power, reactive power and the voltage magnitude at each bus in addition to the frequency of the system. The algorithm is applied to 7-bus, 6-bus and 38-bus systems and the code is run on MATLAB software. The results obtained are compared with time domain simulations carried out by PSIM to assess the effectiveness and the robustness of the investigated algorithm .

Acknowledgment

First things first, my sincere appreciations go for my supervisor Pr.KHELDOUN Aissa for being such a great mentor, and for his consistent support, guidance and for being present throughout the realization of this work.

I would like to thank everyone who ever helped me in my career and supported me in accomplishing this work.

Dedication

In the memory of my father, to my mother, uncle Tayeb, my brothers and my sister and to all my family. I dedicate this work to you and to the dear and special friends I met along the way.

Contents

List of Figures

List of Tables

List of Abbreviations

AC Alternatin Current

CLF Conventional Load Flow

CP Constant Power

CPF Conventional Power FLOW

CPH Combined Heat and Power

CZ Constant Impedance

DEG Distributed Energy Resources

DG Distributed Generator

FES Flywheel Energy Storage

GS Gausse Seidal

HAWT Horizotal Axis Wind Turbine

LC Load controller

LFA Load Flow Analysis

LV Low Voltage

MC Micro source Controller

MG Microgrid

MGCC Microgrid System Central Controller

MGS Modified Gausse Seidal

MNR Modified Newton Raphson

MPPT Maximum Power Point Traking

NR Newton Raphson

PFA Power Flow Analysis

PS Power System

PV Photo-Voltaic

RES Renewable Energy Source

VAWT Vertical Axis Wind Turbine

General introduction

Renewable energy sources, like solar and wind power produce energy intermittently and erratically, which makes it difficult to integrate them widely into the utility system. One alternative is to treat local consumption, traditional sources, storage, and renewable sources as a one unit in the utility grid. Due to its ability to function in both grid-connected and islanded modes, this concept has emerged as one of the most promising technologies to update the current power infrastructure. A microgrid can potentially adapt to end-user and grid requirements more effectively, and it can also help with the installation of a future smart grid.

The electric power system is a complicated system that necessitates careful planning and operation. A power flow analysis is the initial step in constructing a (future expansion of) power system. By measuring the voltage magnitude and angle of each bus in the network, a power flow study computes the flow of electrical power through a system. More and more renewable energy sources (RES) are being included into the electric power grid as the demand for electricity rises and RES technology develops. The scattered and erratic character of RES, as well as the power-electronic interfaces of the majority of loads and RES, present difficulties and necessitate changes to the current power system operation methods, including the power flow studies.

The power flow problem can be easily tackled in grid connected MGs by applying conventional power flow (CPF) methods, such as the Newton Raphson and the Gauss-Seidel, these methods are based on the concept of the slack bus, which is used to simulate the utility grid, in this concept the grid frequency is predetermined, and voltage magnitude of the slack bus is assumed constant and a priori known , whereas in islanded mode the consideration of the slack bus, operating at fixed voltage and frequency is not valid thus, the use of conventional power flow analysis in islanded mode is not effective hence , new concepts and algorithms are developed to solve the load flow problem.[1]

This report aim to provide a novel approach to find the steady state solution for the LFA analysis problem. Instead of the time domain solution using PSIM software that uses the dynamic equations to get accurate results, only MATLAB software is used in order to shorten the time needed for the convergence. This method includes the unique characteristics of the islanded microgrid in the conventional LFA, which extends its application to different topologies.

The thesis is organized in four chapters:

Chapter 1 provides a general view on the concept of microgrid in addition components, mode of operation and types of microgrid.

Chapter 2 provides a state of the art, that presents the well-known methods used to solve the same problem.

Chapter 3 describes how the Modified Newton Raphson is derived from the conventional Newton

Raphson, in addition to the equations added.

Chapter 4 presents and discusses the results obtained from the different networks the algorithm was tested on, in addition to a comparison between our results and the PSIM results and other methods results.

Chapter 1

Introduction to the concept of Microgrid

1.1 Introduction

Due to the energy losses, high investment costs, and user disturbances, recent developments in the electric utility industry are encouraging the entry of power generation and energy storage at the distributed level. Thus, MGs are established for power generation especially for communities and regions that have adequate renewable energy resources. But they cannot be considered as a replacement of the national grid.

1.2 History of Electrical Grid

The power grid as we know it began with isolated power generation systems across the word in 1870's. The first alternating current power grid system was installed in 1886 in Greet Barrington, Massachusetts. At the time, the grid was centralized, unidirectional and demand-driven controlled.

By the 1960s, the electrical grid of developed countries had become very large, mature and highly interconnected, with thousands of central generation power station delivering power to major load centers via high capacity power lines. At the end of this century, the majority of the population joined the electrical grid

Through 1970s to the 1990s, growing demand led to increase the number of power stations. In some areas, supplying of electricity especially at peak times could not keep up with this demand resulting in poor power quality including blackouts, power cuts and brownouts. Later on, these peaks were met by an array of ''peak power generators '' that would only be turned on for short period each day.

Since the early 21st century, opportunities to take advantage of improvements in electronic communication technology to resolve the limitations and costs of the electrical grid. In parallel, growing concerns over environmental damage from fossil fired power stations has led to a desire to use large amounts of renewable energy. So the need for more sophisticated control systems became apparent, to facilitate the connection of sources. Thus modern MGs are entering an area of rapid development and evolution. MGs today take on many different configurations, depending on the application and benefits.

Recently, Smart Grids has become common to describe the future power network that will make use of modern information and communication technologies to support a secure and cost-effective and de-carbonized electrical power system. Smart Grids are intelligently controlled active networks that facilitate the integration of distributed generation into the power system

1.3 Definition of Electrical Grid

Electrical grid or power grid is defined as the network which interconnects the generation, transmission and distribution unit. It supplies the electrical power from generating units (producers) to the distributed units (customers). The electrical grid decomposed into three main components shown below in fig1.1.

- **Generation:** There are two types of generation centralized and decentralized. Centralized generation refers to large-scale generation far from consumption. This includes coal, nuclear, natural gas, hydro, wind farms and large solar arrays. Decentralized generation occurs close to consumption, for example rooftop solar

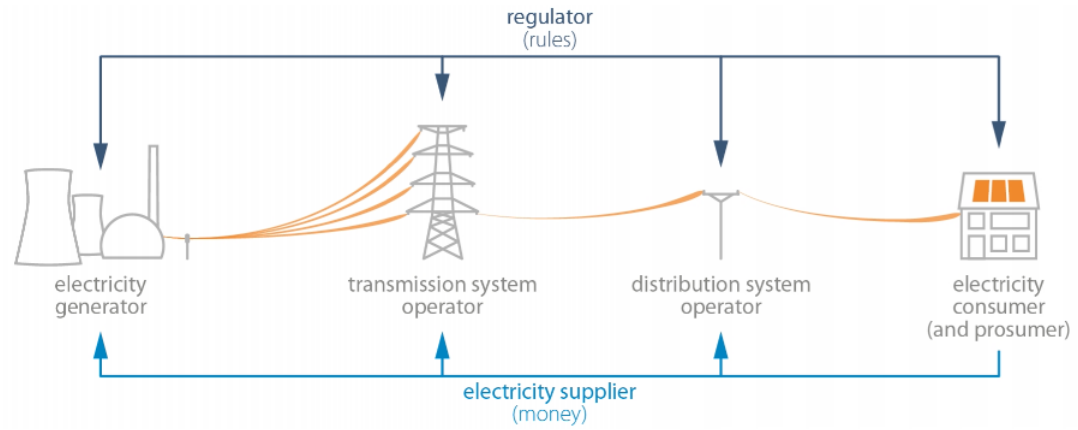

Figure 1.1: Electrical system diagram.

‘

- **Transmission and Distribution:** Transmission includes transformers, substations and power lines that transport electricity from where it is generated to points of consumption. At the point of generation, substations contain transformers that step-up the voltage of electricity so that it can be transmitted. When it arrives at points of consumption, another substation is found to step down the voltage for end-use consumption
- **Consumption:** There are various types of consumers: industrial, commercial and residential consumers.

1.4 Definition of Microgrid

The U.S. Department of Energy has provided the following definition of Microgrids in [2].

"A Microgrid, a local energy network, offers integration of distributed energy resources (DGs) with local elastic loads, which can operate in parallel with the grid or in an intentional island mode to

provide a customized level of high reliability and resilience to grid disturbances. This advanced, integrated distribution system addresses the need for application in locations with electric supply and/or delivery constraints, in remote sites, and for protection of critical loads and economically sensitive development."

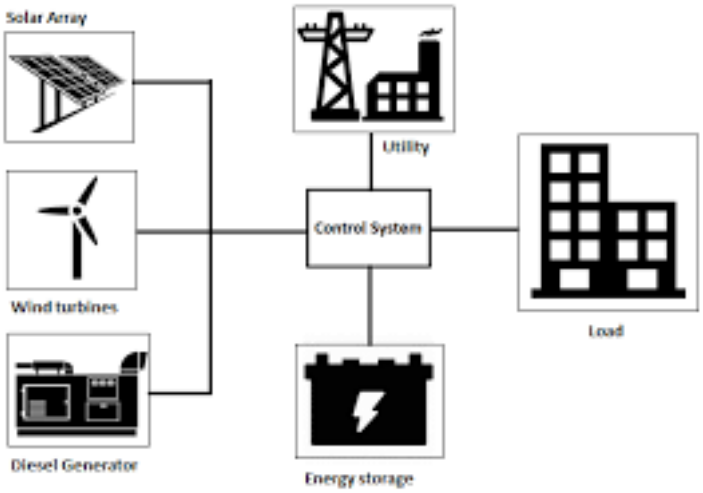

Figure 1.2: Microgrid system topology.

To put it another way, microgrids are small grids that are characterized as low voltage distribution networks that include multiple distributed generators, energy storage systems, and programmable loads that can run either interconnected or isolated from the large power-grid, and can be collectively treated by the grid as controllable load or generators.[3]

The MG includes micro-resources like PV arrays, wind generators, fuel cells, micro-turbines, biomass, geothermal, steam or gas turbines. The storage devices in MGs can include flywheels, energy capacitors (super capacitors), and batteries. The role of the energy storage devices in MG is to strike a balance between energy generation and consumption especially during sudden changes in load or generation.

1.5 Microgrid Physical Structure

1.5.1 Distributed Generators

- **Solar PV:** solar PV is a technology that converts sunlight into direct current electricity by using semi-conductors. Typically, PV cells are pre-wired in series to form the PV module. Multiple modules can be wired together to form an array, which can be scaled up or down depending on the power needed. PV cells can be made from various semi-conductor materials but the most commonly used material today is silicon.
- **Wind turbine:** a wind turbine is a type of electric power generator which converts the kinetic energy of the wind into electrical energy. The wind energy is a result of the difference in atmospheric pressure from one region to another; this energy depends on:
  - The amount of air (Volume)
  - The speed of air (Velocity)

  - The mass of air (Density)

  Wind turbines fall into one of two categories: Horizontal axis wind turbines (HAWTs) and vertical axis wind turbines (VAWTs). HAWTs are the more common type.

- **Fuel cells:** a pollution free electrical generation technology that convert the chemical energy of a fuel directly into electricity. The source fuel could be almost anything that can be oxidized, including hydrogen, methane, propane, methanol, diesel fuel or gasoline. In many respects, a fuel cell resembles a battery, but over a much longer period of time it can supply electrical energy. For this reason, they have been used for decades in space probes, satellites, and manned spacecraft. Nowadays, fuel cells aremostly used in utility power plants, hospital and cars.

1.5.2 Energy Storage Systems

Modern storage systems are unique in that they are very fast responding resources that can both generate and absorb power and, in some cases, regulate real and reactive power quality in an electric distribution system. These capabilities allow storage to serve a variety of roles within a microgrid for instances where customers have a need for uninterrupted islanding, have no on-site generation, or need to supplement the on-site generation that exists in their distribution system.[4]

- **Flywheel energy storage Systems:** flywheel refers to a rotating mass that stores energy in the form of kinetic energy. It can serve as a short-term backup power source when the main energy source fails. The FES has been deployed in many applications, which include—but are not limited to—space systems, telecommunications, and data centers.[5]

- **Energy storage super-capacitors:** it is an electrochemical device, so the energy storage processes are reversible with no chemical reactions. Therefore, the super-capacitor can repeated charge and discharge hundreds of thousands of times. Its power density is 10-100 times more than that of conventional batteries, so it applies to short-term high power output; it could complete the process of charging tens of seconds to minutes due to its fast charging ability, without testing whether it is full, and its over-charge is risk free; it has long life and low-temperature performance. Hence, using super-capacitor as the energy storage device is ideal for applications in a variety of systems.

- **Batteries:** they are electrochemical energy storage devices. There are different forms of batteries: lithium-ion, lead acid, sodium, and others designed to meet specific power and duration requirements. They allow storing the excess of renewable energy for later use to ensure continuity of supply. The main disadvantage for a battery is its short lifespan.

1.6 Types of Microgrids

1.6.1 AC Microgrid

AC microgrid structure is shown in Fig 1.3, DER's are connected to the loads via an AC bus bar and power electronics devices.

This architecture is distinguished by the benefits of having a strong fault management capability and being able to adjust voltage levels simply through the use of transformers. The microgrid uses a variety of protection mechanisms to identify and handle faults when it is operating autonomously.

However, it has several disadvantages, like the requirement for distributed generation synchronization or the circulation of reactive power that increases power losses in the transmission system.

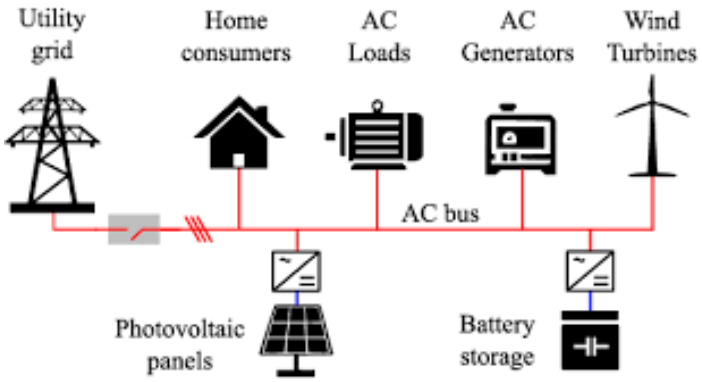

Figure 1.3: AC Microgrid structure.

1.6.2 DC Microgrid

In DC microgrid, DERs and loads are connected to DC bus through power electronic devices. Besides, DC microgrid is connected to the main grid through an inverter, as shown in Fig 1.4 DC microgrid includes DC power sources and loads are more economical.

In fact, these microgrids have been proposed to avoid losses from converting power between DC and AC because various distributed generation sources, such as solar photovoltaic (PV), fuel cells, batteries, etc., as well as various loads, such as lighting, heating, ventilation, etc., output or accept DC power.

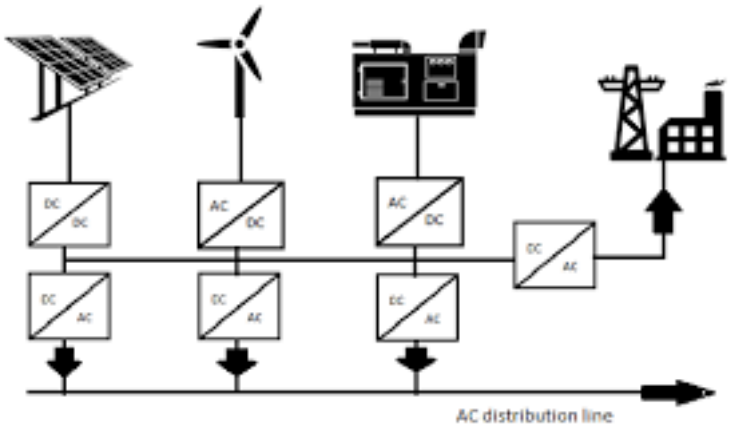

Figure 1.4: DC Microgrid diagram.

It should be noted that losses on conventional AC-type systems typically range from 5% to 15% of power generation and include the cables, conversion stages (from AC to DC), and losses due to skin effects and reactive power flow. As a result of the decreased losses, DC microgrids require less cooling and ventilation equipment since less energy is lost as heat during the conversion process, which is important in applications with high power demands and multiple DC-type sources.

It is worth mentioning that despite the profound benefits mentioned above, Their widespread application is restricted by a few problems. The major of these is the lack of standardization, unlike the low AC

voltage in home appliances which we know operates at level of 230 V, The DC homes does not have such standards. However the efforts to make such standardization possible increased these last few years, proposing two Dc voltage levels for DC buildings, these being 380V for higher load application and 24V or 48 V DC for lower load applications.

1.6.3 Hybrid AC/DC Microgrid

A third option, which has attracted a lot of attention lately, is the hybrid AC/DC microgrids. This configuration combines the advantages of AC and DC architectures as the two sub-networks are connected with the same distribution grid enhancing the integration of both AC and DC based distributed generation resources, energy storage devices and loads. As such, they pose an efficient way for the increased penetration of renewable energy technologies, batteries and even electric vehicles without the need for great modifications, hence with a reduced capital cost. A typical AC/DC microgrid is depicted in Fig 1.5.

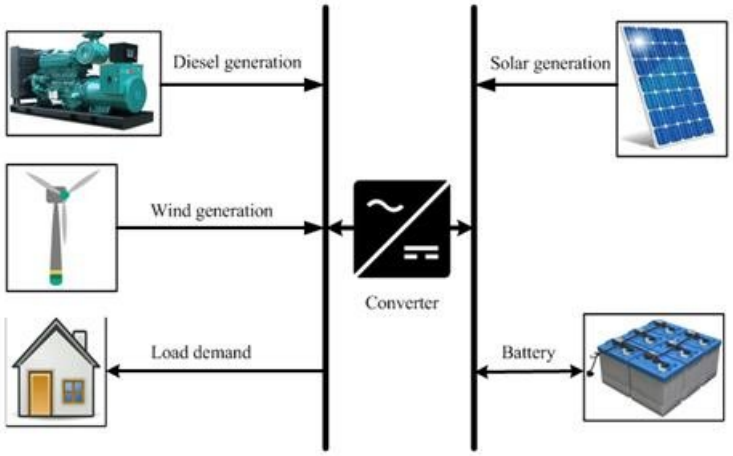

Figure 1.5: Hybrid Microgrid diagram.

As it can be observed in fig 1.5, in a hybrid AC/DC microgrid, AC-type units such as wind turbines and AC loads are connected to an AC bus, while DC-type units such as solar PV, electric vehicles, energy storage devices and DC loads are connected to DC bus bar. The two sub grids are interconnected through the so-called interlinking converter; this can be one or multiple depending on their ratings and those of the sub grids. It is a bidirectional converter which, through its special controllability, performs multiple functions essential for the optimal operation of hybrid AC/DC microgrids. As an example, power sharing through the two sub grids is enabled via a droop control strategy implemented in the interlinking converter.

1.7 Control of a Microgrid

The MG system is controlled and managed using programmable logic controllers in order to achieve the needed flexibility. The MG controllers consists of:

- Micro Source Controllers (MC) and Load Controllers (LC).
- Microgrid System Central Controller (MGCC).

– Distribution Management System (DMS). These controller are used to execute the process in automated process. In order to ensure that new and current assets can communicate with one another, it is essential for MG setup to adhere to commonly used industrial protocols that are already present in automation devices. Examples of these devices are PLCs and feeder protection relays.

Control methods are made based on the manner of operation of a microgrid.

1.7.1 Grid Connected Mode

When operating in grid connected mode or "on-grid," DG is coupled to the utility grid via STS at the Point of Common Coupling (Static Transfer Switch). The MGCC determines how much active and reactive power a DG should inject. The local devices are under the control of the MCs and LCs, which receive directives from the MGCC. PQ control is used in this mode to control active and reactive power from the inverter. Communication between MGCC, MCs, and LCs is to convey tiny amounts of information relating to set points of active and reactive power, reference voltage and frequency, etc.

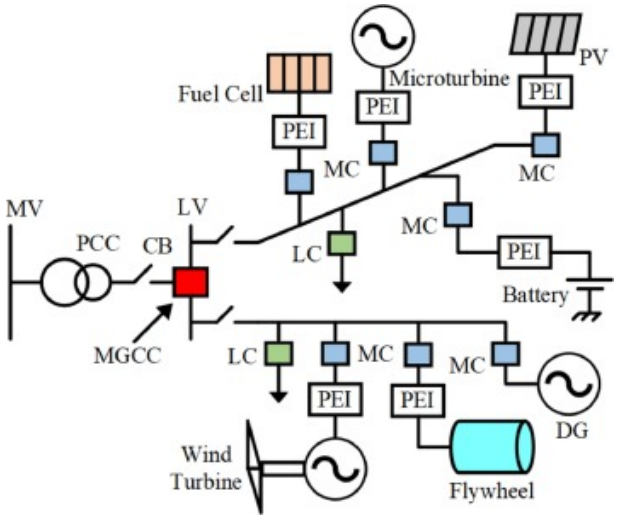

Figure 1.6: Microgrid Automation and control.

1.7.2 Islanded Mode

In this mode the microgrid operates independently, it switches to this mode for maintenance, power outages, or financial considerations. Using centralized or decentralized control, inverters functioning as voltage sources can receive the voltage and frequency set points they need.[6]

1.8 Characteristics of Microgrid

Microgrid is characterized with some valuable aspect which can be resumed as follow:

Independence: MG can operate in islanded mode. In autonomous operation, MG is capable of balancing generation and load. Besides, it can keep system voltage and frequency in defined limits with adequate controls.

Flexibility: The expansion and growth rate of MGs do not need to follow any precise forecasts. According to operation modes, MGs can operate in different modes. Connecting to the main grid is optional.

Stability: MG can operate stably during nominal operating modes and transient events, no matter whether the larger grid is up or down (Additional research is required).

Interactivity: MGs are compatible with the main grid. They can support the main grid if it is necessary and the main grid can also supply for MGs.

Efficiency: The utilization of DERs optimization and manage loads by using centralized as well as distributed MG controller is the way to make energy management goals optimization.[7]

Expanse: MGs can grow easily by adding more distributed energy resources (DERs) and loads. It is easier than expand the traditional grid.

1.9 Conclusion

This chapter presents fundamental introduction of microgrid concept with its components and different operation modes. Moreover, active distribution networks and required control and source infrastructures have been introduced. The most widely used renewable energy sources such as wind turbines and solar PV plants have been presented in brief following the active distribution networks.

The micro-grid can be considered as a controlled cell of the power system for the utility purpose whereas, to the consumer the micro-grid can be planned to meet their special requirements such as, enhancement of local reliability, reduction of feeder loses, and local voltages support. Microgrids are a compact version of traditional power system connection multiple distributed sources to multiple loads, which draws the interest of power system planners as they can be of great importance when it comes to electrifying remote areas.

Chapter 2

Review of Microgrid Load Flow Methods

2.1 Introduction

This chapter demonstrates the other used solutions to solve the load flow analysis for islanded microgrid. Each method has its own advantages and disadvantages, and serves to solve specific systems. The optimal solution is the one that can be applied to a large number of benchmarks, coverges in a short period of time in addition to having the most accurate results without relying on external softwares.

2.2 Gausse Seidal Technique

Gausse Seidal is widely used for the Conventional Load Flow systems. However it cannot be implemented directly to solve the power flow problem in microgrids. For this matter the following method is proposed found in [8].

2.2.1 Modified Gausse Siedal

This method is solved in two steps. The first is the same as conventional GS method but with some modifications. The second solves the problem for the angular frequency ω.

The first step starts with the assumption of voltages to be$1\angle 0$ but in this case bus1 (conventionally treated as slack bus) is also a variable. Furthermore, frequency is also assumed to be 1 p.u. which is calculated in second step of MGS. So there are two extra variables involved in MGS calculations. The state vector is given by :

$$X = \begin{bmatrix} V \\ \omega \end{bmatrix} \tag{2.1}$$

where ω is the system angular frequency. V is the complex voltage vector including bus1. The flowchart of the proposed method is shown in Fig 2.1 below. To solve the first step for voltages at all

buses the conventional GS voltage expression is used which is given by

$$V_k^{i+1} = \frac{1}{Y_{kk}} \left[\frac{P_k - JQ_k}{(V_k^i)^*} - \sum_{n=1}^{k-1} Y_{kn} V_n^{i+1} - \sum_{n=k+1}^{N} Y_{kn} V_n^i \right] \tag{2.2}$$

$$Q_k^{i+1} = -\Im \left\{ (V_k^i)^* \left(\sum_{n=1}^{k-1} Y_{kn} V_n^{i+1} + \sum_{n=k}^{N} Y_{kn} V_n^i \right) \right\} \tag{2.3}$$

In order to finish the first step and update the voltages, the Active and Reactive power of the droop buses are calculated as shown in step 4 of the flowchart below 2.1.

The second step of the of the MGS method involves the calculation of the frequency, using the sum of the DG's power that equals the total load in addition to the losses of the system. The equation shown in step 9 in Fig 2.1 is used to update the angular frequency.

The proposed method to solve the power flow problem showed an accurate modelling of the microgrid operation, where DG's share the load demands keeping the system frequency and voltages within specified limits. However, eventhough the the Gausse Seidal technique is simpler, its use can be criticized because of :

- The convergence depends on many factors such as: the initial solutions, the acceleration factor, the tolerance limit, the slack bus selection, level of accuracy of results needed.
- Slow rate of convergence resulting a large number of iterations.
- Increasing in the number of iterations with increase in the number of buses.

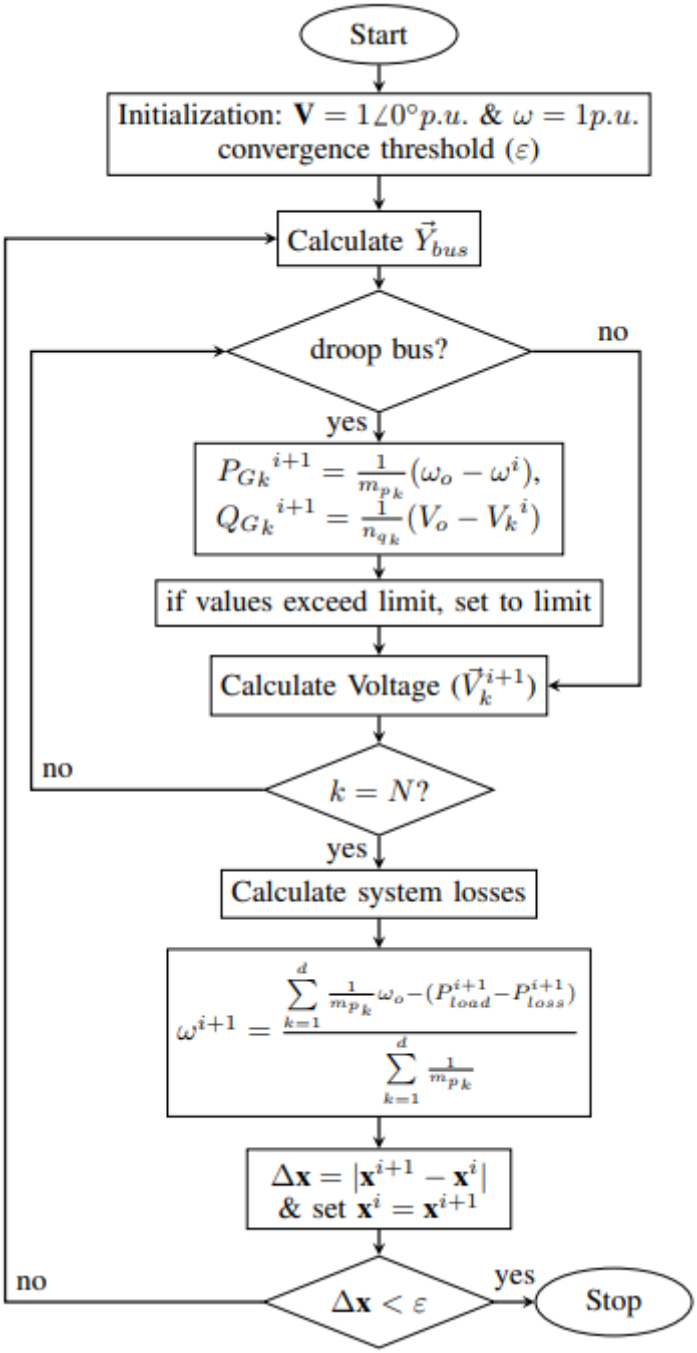

Figure 2.1: Modified Gausse Seidal flowchart.

2.3 Newton Raphson Technique

Both off the following algorithms were developed and published by the same team of researchers. The first is tested on the 7-bus system, the second was upgraded and tested in a larger system of 18 buses. CLF mathematical formulas are used then the equilibrium operating points of the islanded MG are determined through an iterative procedure.

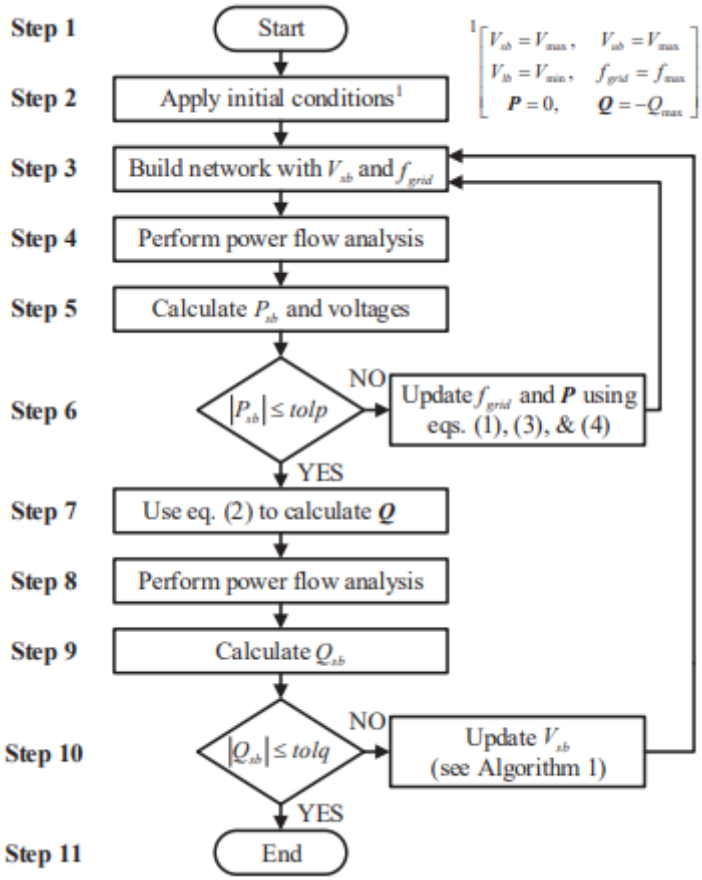

Figure 2.2: Proposed method flowchart.

2.3.1 First algorithm

The following method consist of two stages as shown below in fig 2.2, The inner loop is used to calculate fgrid, while the outer loop defines V_{sb}. At the first step, the initial conditions are determined. Afterwards, line and load impedances are calculated at fgrid and a power flow analysis is performed. This power flow aims to calculate network voltages and the active power flowing through the slack bus P_{sb}. If the absolute value of P_{sb}, i.e., $|P_{sb}|$, is greater than a predefined tolerance Tolp, DG units must adjust their injected active power by a ΔP_i amount. Following this approach, P_{sb} is allocated to all DG units in order to zero the active power flow through the slack bus. ΔP_i amounts are modified accordingly with the droop control equations. After that P is updated and a new fgrid is derived using droop equations then LFA is conducted again. This process is repeated until Tolp is matched, then the algorithm moves to adjusting the V_{sb} using the binary search algorithm.

The disadvantages of this algorithm is:

- It regulates frequency for each update of slack bus voltage. In addition to updating the values outside the the load flow using the binary search algorithm, which can take longer iterations to converge.
- It does not use one environment to build the whole algorithm at once. The load flow is done externally causing more unnecessary wasted time.

2.3.2 Second algorithm

The following algorithm presented below in Fig 2.3 consists of three nested loops. The third loop was added to simulate closely the Q-V droop control, with the aim to eliminate the numerical oscillations of the injected power and network voltage which may lead to convergence issues in extended networks with high penetration of DG's.

The added loop compares all the node voltages between the last two iterations performed. If tolv criterion is satisfied, the algorithm proceeds to Step-12, otherwise the algorithm moves back to Step-6 and new reactive power injections are computed.

The algorithm is tested on an 18-bus microgrid with six distributed generators and five loads in which their values were not mentioned. The algorithm is build in MATLAB and OpenDSS software. The former is used to implement the flowchart of Fig 2.3, while the latter is utilized as a phase-domain power flow solver.

The use of OpenDSS assured the convergence even in a weakly meshed system like the 18-bus system found in [1], which did not converge when MATLAB only was used. However the algorithm did converge with the 7-bus system without the use of OpenDSS. Comments on both algorithms: Even though the second algorithm is extended and upgraded; the two algorithms shares the same structure. They both rely on other softwares like OpenDSS to perform the load flow, then the equilibrium operating points of the microgrid are found through in iterative procedure.

Both methods were tested solely in MATLAB and discussed in last year thesis [9], they showed interesting results regarding the 7-bus system because of the algorithm's ability to nullify the slack bus power with high accuracy, mimicking the behaviour of a microgrid. However this method presents two main problems the first being the time consumption due to the use of openDSS and the outside update. In addition to the ineffectiveness of the algorithm when used solely in MATLAB with weakly meshed systems. The second is the inability to observe the exact procedure in which the LFA is conducted, hence it cannot be modified or upgraded like we have seen in the MGS method.

2.4 Meta-heuristic techniques

Instead of using an external software to solve the LFA problem, Evolutionary methods such as Practical Swarm Optimization and Differential Evolution are used.

2.4.1 Practical Swarm Optimization

PSO is smart optimization technique that has been inspired by the social and cooperative behavior displayed by various species like birds, fish and human beings.

The proposed algorithms use the PSO technique to the load flow calculation taking into account the droop characteristic of the DGs.

The power flow equations are as follows:

$$Q_k = \sum_{n=1}^{N} |V_k||V_n| \left(G_{kn} sin(\theta_k - \theta_n) - B_{kn} cos(\theta_k - \theta_n)\right) \tag{2.4}$$

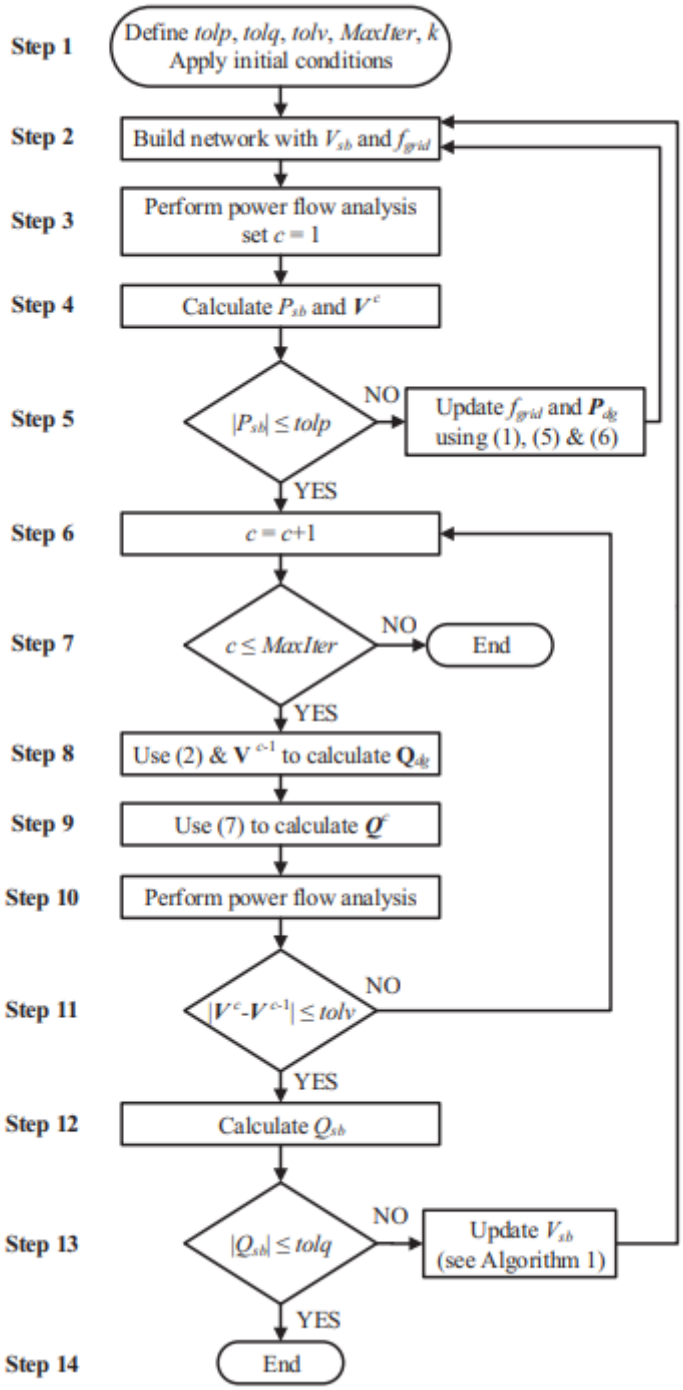

Figure 2.3: Second algorithm flowchart.

$$P_k = \sum_{n=1}^{N} |V_k||V_n| \left(G_{kn} sin(\theta_k - \theta_n) + B_{kn} cos(\theta_k - \theta_n)\right) \tag{2.5}$$

2.4.2 Differential Evolution

Differential Evolution is a population based optimization algorithm. DE starts with a population of candidate solutions, the working of DE depends on the manipulation and efficiency of three main operators: initialization, mutation, recombination and selection.

2.4.3 Discussion

For both methods two algorithms were used. The one first being the exact same algorithm shown in the flowchart in Fig 2.2 where a cascaded optimization is performed.

The second algorithm uses only one loop(Single Optimization). Where the active and reactive powers of the slack bus are calculated using Eq 2.5 and Eq 2.4 but the value used in the mismatch is given by $\Delta S^2 = \Delta P^2 + \Delta Q^2$

- In case, where ΔS^2 is higher than the tolerance the algorithm moves back to step one to repeat the calculations.
- In case, where less than the tolerance the algorithm displays the final value of the frequency, generated active and reactive powers and the voltage magnitudes and angles.
- Both algorithms and the results of the 7-bus and 38-bus systems are shown in details in [10].

2.5 Conclusion

In this chapter several load flow solution techniques were presented. Although they are different they share the same core idea of integrating droop control equations with the conventional load flow techniques through an iterative procedure or via including it directly inside the CLF technique.

Chapter 3

Load flow analysis for Microgrid

3.1 Introduction

The power flow problem can be easily solved in a conventional power plant using newton raphson or any other techniques. These methods rely on the presence of the slack bus that imitates the behavior of a large synchronous machine, providing/absorbing the deficit/surplus of active. In this concept, the grid frequency is predetermined, while the voltage magnitude of the slack bus is assumed to be constant and priory known. [1]

Conventional load flow techniques cannot be applied directly to an islanded microgrid. Due to the limited power generated by each distributed generator, which are incapable of satisfying the transmission line losses alone, Hence no slack bus can be present in the network. In addition to the variable frequency of the microgrid that affects the networks reactances.

3.2 Conventional load flow with Newton Raphson

The Newton-Raphson method is being widely used which is more reliable but has higher memory requirements. The use of sparsity programming and optimal ordering has reduced memory requirements and increased the popularity of the method.[11]

To solve a power flow problem the types of buses present in the system must be identified.

3.2.1 Defining the buses in the system

There are three categories of buses in a system :

PV bus: Generation bus is where the generator is connected to, the bus has two known quantities are the voltage and the active power. Therefore the unknown quantities are the reactive power and the voltage angle.

PQ bus: This bus is where the load is connected. The active and reactive power are known, the voltage magnitude and the angle need to be found.

Slack bus : This bus is connected to a generator but the active power and reactive power are not known because the losses of transmission lines are not yet known and assigned to this bus. Though

the voltage level is assumed to be constant and the angle is set to zero.

Bus type	Known quantities	unknown quantities
PV bus	P ,$\|V\|$	Q,δ
PQ bus	P , Q	$\|V\|$, δ
slack bus	$\|V\|$,δ	P,Q

Table 3.1: Bus clarification of the power system

3.2.2 Problem formulation

In the conventional NR method, the slack bus voltage is fixed at $1\angle 0$ and all the remaining system buses are initialized with a voltage of $1\angle 0$ which will change with each iteration. The active and reactive power mismatch is calculated and through the Jacobian, the voltage magnitude and angle mismatches are determined. The convergence criterion is based on setting a tolerance on the voltage magnitude and angle mismatch [12]. For a system with N buses, the polar form of the power flow equations is given by

$$P_{ck}^{(t)} = |V_k| \sum_{n=1}^{N} |Y_{kn}||V_n| cos(\delta_k - \delta_n - \theta_{kn}) \tag{3.1}$$

$$Q_{ck}^{(t)} = |V_k| \sum_{n=1}^{N} |Y_{kn}||V_n| sin(\delta_k - \delta_n - \theta_{kn}) \tag{3.2}$$

Assuming the first bus to be the slack bus, the calculated values of the real power P_c and reactive power Q_c of the other buses are obtained from eq 3.1 and eq 3.2, respectively; and are compared with the scheduled values to obtain the mismatch matrix Δ as follows

$$\Delta = \begin{bmatrix} P_{inj} - P_c \\ Q_{inj} - Q_c \end{bmatrix} \tag{3.3}$$

The state vector is given by

$$X^t = \begin{bmatrix} \delta^t \\ V^t \end{bmatrix} \tag{3.4}$$

The Jacobian matrix is calculated using

$$J = \left[\begin{array}{ccc|ccc} \frac{\partial P_2}{\partial \delta_2} & \cdots & \frac{\partial P_2}{\partial \delta_N} & \frac{\partial P_2}{\partial V_2} & \cdots & \frac{\partial P_2}{\partial V_N} \\ \vdots & \ddots & \vdots & \vdots & \ddots & \vdots \\ \frac{\partial P_N}{\partial \delta_2} & \cdots & \frac{\partial P_N}{\partial \delta_N} & \frac{\partial P_N}{\partial V_2} & \cdots & \frac{\partial P_N}{\partial V_N} \\ \hline \frac{\partial Q_2}{\partial \delta_2} & \cdots & \frac{\partial Q_2}{\partial \delta_N} & \frac{\partial Q_2}{\partial V_2} & \cdots & \frac{\partial Q_2}{\partial V_N} \\ \vdots & \ddots & \vdots & \vdots & \ddots & \vdots \\ \frac{\partial Q_N}{\partial \delta_2} & \cdots & \frac{\partial Q_N}{\partial \delta_N} & \frac{\partial Q_N}{\partial V_2} & \cdots & \frac{\partial Q_N}{\partial V_N} \end{array}\right] \tag{3.5}$$

In a simpler form

$$J = \begin{bmatrix} J_{11} & J_{12} \\ J_{21} & J_{22} \end{bmatrix} \tag{3.6}$$

The elements of the Jacobian matrix can be evaluated using the power flow equations of active and reactive power as shown below

$$\begin{cases} \frac{\partial P_k}{\partial \delta_k} = \sum_{n=1 n\neq k}^{N} |Y_{kn}||V_n||V_k| sin(\delta_n + \theta_{kn} - \delta_k) \quad n \neq k, \quad Diagonal \\ \\ \frac{\partial P_k}{\partial \delta_k} = -|Y_{kn}||V_n||V_k| sin(\delta_n + \theta_{kn} - \delta_k), \quad n \neq k, \quad off-diagonal \end{cases} \tag{3.7}$$

$$\begin{cases} \frac{\partial P_k}{\partial V_k} = 2|Y_{kk}||V_k| cos(\theta_{kk}) + \sum_{n=1 n\neq k}^{N} |Y_{kn}||V_n| cos(\delta_n + \theta_{kn} - \delta_k), \quad n \neq k \quad Diagonal \\ \\ \frac{\partial P_k}{\partial V_k} = |Y_{kn}||V_k| cos(\delta_n + \theta_{kn} - \delta_k), \quad n \neq k, \quad off-diagonal \end{cases} \tag{3.8}$$

$$\begin{cases} \frac{\partial Q_k}{\partial \delta_k} = \sum_{n=1 n\neq k}^{N} |Y_{kn}||V_n||V_k| cos(\delta_n + \theta_{kn} - \delta_k), \quad n \neq k \quad Diagonal \\ \\ \frac{\partial Q_k}{\partial \delta_k} = -|Y_{kn}||V_n||V_k| cos(\delta_n + \theta_{kn} - \delta_k) \quad n \neq k \quad off-diagonal \end{cases} \tag{3.9}$$

$$\begin{cases} \frac{\partial P_k}{\partial V_k} = -2|Y_{kk}||V_k| sin(\theta_{kk}) - \sum_{n=1 n\neq k}^{N} |Y_{kn}||V_n| sin(\delta_n + \theta_{kn} - \delta_k), \quad n \neq k \quad Diagonal \\ \\ \frac{\partial P_k}{\partial \delta_k} = -|Y_{kn}||V_k| sin(\delta_n + \theta_{kn} - V_k) \quad n \neq k, \quad off-diagonal \end{cases} \tag{3.10}$$

When the Jacobian matrix is obtained the state vector of the next iteration is calculated as follow:

$$X^{t+1} = X^t + J^{-1}\Delta \tag{3.11}$$

As mentioned in the introduction, conventional Newton Raphson technique cannot be applied directly. However it can work if the generation buses are changed into droop buses, in addition to taking into account the changing frequency and the slack bus voltage.

3.3 Droop Control Method

The droop control scheme mimics the operation of the governor and exciter in synchronous generators and determines the output frequency and voltage of DG's according to the active and reactive powers derived from their terminals. This lead to effective power sharing between the distributed generators in an autonomous microgrid. This allows the microgrid to operate stably even at high energy fluctuations. When the power injected exceeds the rated power of the battery inverter The droop control will automatically increase the frequency. the distributed generator inverter will sense the increase in frequency and throttle the injected power. The droop control strategy holds an edge over the other control strategies because no communication among the power converters is required. Thereby the reliability is improved without any restriction on the physical location of the power converters tied to the distributed generators. These generators are usually connected to high voltage lines, which are

also mainly inductive. Consequently, the impedance of the equivalent circuit is considered inductive and the active and reactive powers can be described as follows:

$$P = \frac{EVsin(\alpha)}{X} \tag{3.12}$$

$$Q = \frac{EVcos(\alpha) - V^2}{X} \tag{3.13}$$

3.3.1 System models

The models of the system are an important factor influencing the power flow study of microgrids the distributed generation model and the Y_{bus} model are presented.

3.3.1.1 Distributed generator model

In grid-connected mode, DG's are usually modeled as PV or PQ buses. In islanded mode, since there is no slack bus, it is impossible to model all the DG's as PV or PQ buses. So DG's in islanded microgrids are modeled as droop buses where the voltage and the frequency droop controls are based on the well-known active power-frequency (P/f) and reactive power-voltage (Q/V) droop characteristics as it is shown in the figure below The active and reactive powers are adjusted according

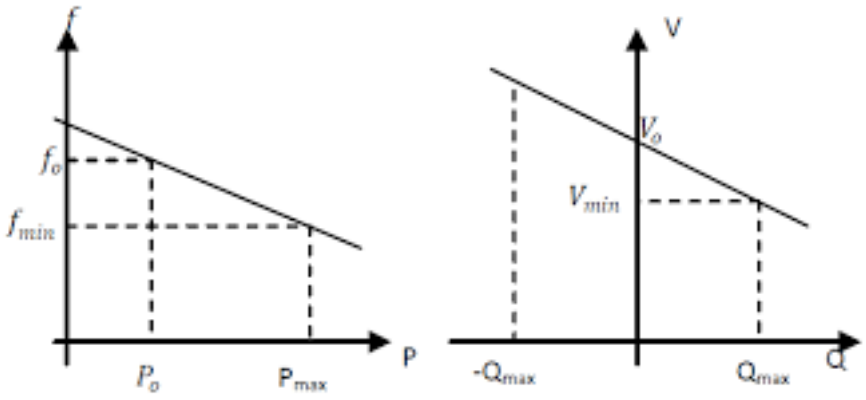

Figure 3.1: P/f and Q/V droop characteristics of a DG

to linear characteristics, based on the following control equations:

$$\begin{cases} f = f_0 - m_i(P_G - P_0) \\ V = V_0 - n_i(Q_G - Q_0) \end{cases} \tag{3.14}$$

- f_0: is the nominal system frequency;
- V_0 is the nominal system voltage amplitude;
- m and n: are the droop frequency and amplitude coefficients, respectively;
- P_0 and Q_0 : are the nominal output power, they are usually set to zero.

3.3.1.2 Y_{bus} model

For an N bus system, Y_{bus} is defined as a matrix representing the nodal admittance of all buses in a system. In case of droop based control of DG's in an islanded microgrid, the system frequency

cannot be treated as a fixed parameter. Since the system frequency affects the line reactance, it should be taken into account for the Y_{bus} calculation. Therefore, for a system with N buses, Y_{bus} will be a function of the system frequency as follows :

$$Y_{bus}(\omega) = \begin{bmatrix} Y_{11}(\omega) & Y_{12}(\omega) & \dots & Y_{1N}(\omega) \\ Y_{21}(\omega) & Y_{22}(\omega) & \dots & Y_{2N}(\omega) \\ \vdots & \vdots & \ddots & \vdots \\ Y_{N1}(\omega) & Y_{N2}(\omega) & \dots & Y_{NN}(\omega) \end{bmatrix} \tag{3.15}$$

Where

$$Y_{kn}(\omega) = \begin{cases} -Z_{kn}(\omega)^{-1} & \forall k \neq n \\ \\ \sum_{n=1, n\neq k}^{N} Z_{kn}(\omega)^{-1} & \forall k = n \end{cases} \tag{3.16}$$

3.4 Modified Newton Raphson

This proposed method includes the changing frequency and the slack bus voltage into the state vector. In addition to adding the difference between the power generated and the power consumed(both active and reactive). This way the Newton Raphson vectors are reintroduced as follows:

$$X' = \begin{bmatrix} \delta \\ V \\ \omega \\ V1 \end{bmatrix} \tag{3.17}$$

$$\Delta' = \begin{bmatrix} P_{inj} - P_c \\ Q_{inj} - Q_c \\ P_{tot} - P_{sys} \\ Q_{tot} - Q_{sys} \end{bmatrix} \tag{3.18}$$

Where P_{sys} is the sum of the generated active power and is represented as

$$P_{sys} = \sum_{k=1}^{d} P_{Gk} \tag{3.19}$$

And the active power generated by each single DG is given as a function of the angular frequency as

$$P_{Gk} = \sum_{k=1}^{d} \frac{\omega_0 - \omega}{m_k} \tag{3.20}$$

Similarly the sum of reactive power generated can be represented as

$$Q_{sys} = \sum_{k=1}^{d} Q_{Gk} \tag{3.21}$$

And the reactive power generated by a single DG is given as a function of the droop bus voltage as

$$Q_{Gk} = \sum_{k=1}^{d} \frac{|V_0| - |V_k|}{n_k} \tag{3.22}$$

Where d is the number of droop buses. The other added elements P_{tot} and Q_{tot} are the total power demand of the system load and losses

$$P_{tot} = P_{load} + P_{loss} \tag{3.23}$$

$$Q_{tot} = Q_{load} + Q_{loss} \tag{3.24}$$

Where P_{loss} and Q_{loss} are calculated as

$$P_{loss} = \frac{1}{2}\sum_{k=1}^{N}\sum_{n=1}^{N}\Re\{Y_{kn}(V_k^* V_n + V_n^* V_k)\} \tag{3.25}$$

$$Q_{loss} = \frac{-1}{2}\sum_{k=1}^{N}\sum_{n=1}^{N}\Im\{Y_{kn}(V_k^* V_n + V_n^* V_k)\} \tag{3.26}$$

As a result of the state and the mismatch vectors increasing in size, the Jacobian matrix increased in size as well.

$$J' = \begin{bmatrix} J_{11} & J_{12} & J_{13} & J_{14} \\ J_{21} & J_{22} & J_{23} & J_{24} \\ J_{31} & J_{32} & J_{33} & J_{34} \\ J_{41} & J_{42} & J_{43} & J_{44} \end{bmatrix} \tag{3.27}$$

Next, replacing each vector by its corresponding value to get the full modifies Jacobian matrix

$$J' = \left[\begin{array}{ccc|ccc|c|c} \frac{\partial P_2}{\partial \delta_2} & \cdots & \frac{\partial P_2}{\partial \delta_N} & \frac{\partial P_2}{\partial V_2} & \cdots & \frac{\partial P_2}{\partial V_N} & \frac{\partial P_2}{\partial \omega} & \frac{\partial P_2}{\partial V_1} \\ \vdots & \ddots & \vdots & \vdots & \ddots & \vdots & \vdots & \vdots \\ \frac{\partial P_N}{\partial \delta_2} & \cdots & \frac{\partial P_N}{\partial \delta_N} & \frac{\partial P_N}{\partial V_2} & \cdots & \frac{\partial P_N}{\partial V_N} & \frac{\partial P_N}{\partial \omega} & \frac{\partial P_N}{\partial V_1} \\ \hline \frac{\partial Q_2}{\partial \delta_2} & \cdots & \frac{\partial Q_2}{\partial \delta_N} & \frac{\partial Q_2}{\partial V_2} & \cdots & \frac{\partial Q_2}{\partial V_N} & \frac{\partial Q_2}{\partial \omega} & \frac{\partial P_N}{\partial V_1} \\ \vdots & \ddots & \vdots & \vdots & \ddots & \vdots & \vdots & \vdots \\ \frac{\partial Q_N}{\partial \delta_2} & \cdots & \frac{\partial Q_N}{\partial \delta_N} & \frac{\partial Q_N}{\partial V_2} & \cdots & \frac{\partial Q_N}{\partial V_N} & \frac{\partial Q_N}{\partial \omega} & \frac{\partial Q_N}{\partial V_1} \\ \hline \frac{\partial P_{sys}}{\partial \delta_2} & \cdots & \frac{\partial P_{sys}}{\partial \delta_N} & \frac{\partial P_{sys}}{\partial V_2} & \cdots & \frac{\partial P_{sys}}{\partial V_N} & \frac{\partial P_{sys}}{\partial \omega} & \frac{\partial P_{sys}}{\partial V_1} \\ \hline \frac{\partial Q_{sys}}{\partial \delta_2} & \cdots & \frac{\partial Q_{sys}}{\partial \delta_N} & \frac{\partial Q_{sys}}{\partial V_2} & \cdots & \frac{\partial Q_{sys}}{\partial V_N} & \frac{\partial Q_{sys}}{\partial \omega} & \frac{\partial Q_{sys}}{\partial V_1} \end{array}\right] \tag{3.28}$$

The first four sub-matrices $[J_{11}J_{12}J_{21}J_{12}]$ are the Jacobian matrix of the regular Newton Raphson. The detailed expressions of the added partial terms are:

- **Elements of J_{13}:**

$$\frac{\partial P_{ck}}{\partial \omega} = |V|\sum_{n=1}^{N}\frac{\partial |Y_{kn}|}{\partial \omega}|V_n| cos(\delta_k - \delta_n - \theta_{kn}) + \frac{\partial |\theta_{kn}|}{\partial \omega}|Y_{kn}| sin(\delta_k - \delta_n - \theta_{kn}) \tag{3.29}$$

- **Elements of J_{23}:**

$$\frac{\partial Q_{ck}}{\partial \omega} = |V| \sum_{n=1}^{N} \frac{\partial |Y_{kn}|}{\partial \omega} |V_n| sin(\delta_k - \delta_n - \theta_{kn}) - \frac{\partial |\theta_{kn}|}{\partial \omega} |Y_{kn}| cos(\delta_k - \delta_n - \theta_{kn}) \tag{3.30}$$

Where:

$$\frac{\partial |Y_{kn}|}{\partial \omega} = -\frac{X_{kn}^2/\omega}{(R_{kn}^2 + X_{kn}^2)^{(\frac{3}{2})}} \tag{3.31}$$

$$\frac{\partial |\theta_{kn}|}{\partial \omega} = -\frac{X_{kn}/(\omega R_{kn}}{1 + (X_{kn}/R_{kn})^2} \tag{3.32}$$

- **Elements of J_{14}:**

$$\frac{\partial P_{ck}}{\partial V_1} = |V_k||Y_{k1}| cos(\delta_k - \delta_1 - \theta_{k1}) \tag{3.33}$$

- **Elements of J_{24}:**

$$\frac{\partial Q_{ck}}{\partial V_1} = |V_k||Y_{k1}| sin(\delta_k - \delta_1 - \theta_{k1}) \tag{3.34}$$

- **Elements of J_{31}:**

$$\frac{\partial P_{sys}}{\partial \delta_k} = 0 \tag{3.35}$$

- **Elements of J_{32}:**

$$\frac{\partial P_{sys}}{\partial |V_k|} = 0 \tag{3.36}$$

- **Elements of J_{33}:**

$$\frac{\partial P_{sys}}{\partial \omega} = \sum_{k=1}^{d} \frac{-1}{m_k} \tag{3.37}$$

- **Elements of J_{34}:**

$$\frac{\partial P_{sys}}{\partial |V_1|} = 0 \tag{3.38}$$

- **Elements of J_{42}:**

$$\frac{\partial Q_{sys}}{\partial |V_k|} = \begin{cases} \frac{-1}{n_k}, & \text{if bus k is a droop bus} \\ 0 & otherwise \end{cases} \tag{3.39}$$

- **Elements of J_{44}:**

$$\frac{\partial Q_{sys}}{\partial |V_1|} = \begin{cases} \frac{-1}{n_1}, & \text{if bus 1 is a droop bus} \\ 0 & \text{otherwise} \end{cases} \tag{3.40}$$

- **Elements of J_{41}:**

$$\frac{\partial Q_{sys}}{\partial \delta_k} = 0 \tag{3.41}$$

- **Elements of J_{43}:**

$$\frac{\partial Q_{sys}}{\partial \omega} = 0 \tag{3.42}$$

Once the modified Jacobian matrix is evaluated the new values of the state vector X' are updated the same way as X but with different variables

$$X'^{t+1} = X'^{t} + J'^{-1}\Delta' \tag{3.43}$$

A more detailed equations is shown bellow:

$$\begin{bmatrix} \delta^{t+1} \\ V^{t+1} \\ \omega^{t+1} \\ V_1^{t+1} \end{bmatrix} = \begin{bmatrix} \delta^{t} \\ V^{t} \\ \omega^{t} \\ V_1^{t} \end{bmatrix} + \begin{bmatrix} J_{11} & J_{12} & J_{13} & J_{14} \\ J_{21} & J_{22} & J_{23} & J_{24} \\ J_{31} & J_{32} & J_{33} & J_{34} \\ J_{41} & J_{42} & J_{43} & J_{44} \end{bmatrix}^{-1} \begin{bmatrix} P_{inj} - P_c \\ Q_{inj} - Q_c \\ P_{tot} - P_{sys} \\ Q_{tot} - Q_{sys} \end{bmatrix} \tag{3.44}$$

The algorithm is based on the Modified Newton Raphson technique the steps taken are explained below :

Step1:

In this step the initial conditions are set. In addition to the maximum values of the voltage and frequency.

Stpe2:

The Y_{bus} is calculated depending on the frequency of the system.

Step3:

The active power and reactive power of each bus(except the slack bus) are calculated using the equations of the CLF NR method shown in Eq 3.1 and 3.2.

Step4:

Using $|V|$, ω and the droop equations given in Eq 3.20 and 3.22 P_{Gk} and Q_{Gk} of each droop bus is calculated. Then the P_{sys} and Q_{sys} are calculated using Eq 3.19 and 3.21.

Step6:

The losses in the transmission lines is evaluated using the Eq 3.25 and 3.26 at the given frequency and voltages.

Step7:

This step evaluates the power consumed by the load if the impedance of the loads is given instead of the power.

Step8:

The overall power consumed by the system is evaluated to be compared with P_{sys} and Q_{sys} afterwards.

Step9:

The modified mismatch matrix is computed using equation Eq 3.18. If the values are almost zero, it means the algorithm has converged and found the suitable values of the voltage levels, angles, frequency of the system and the slack bus voltage level.

Step10:

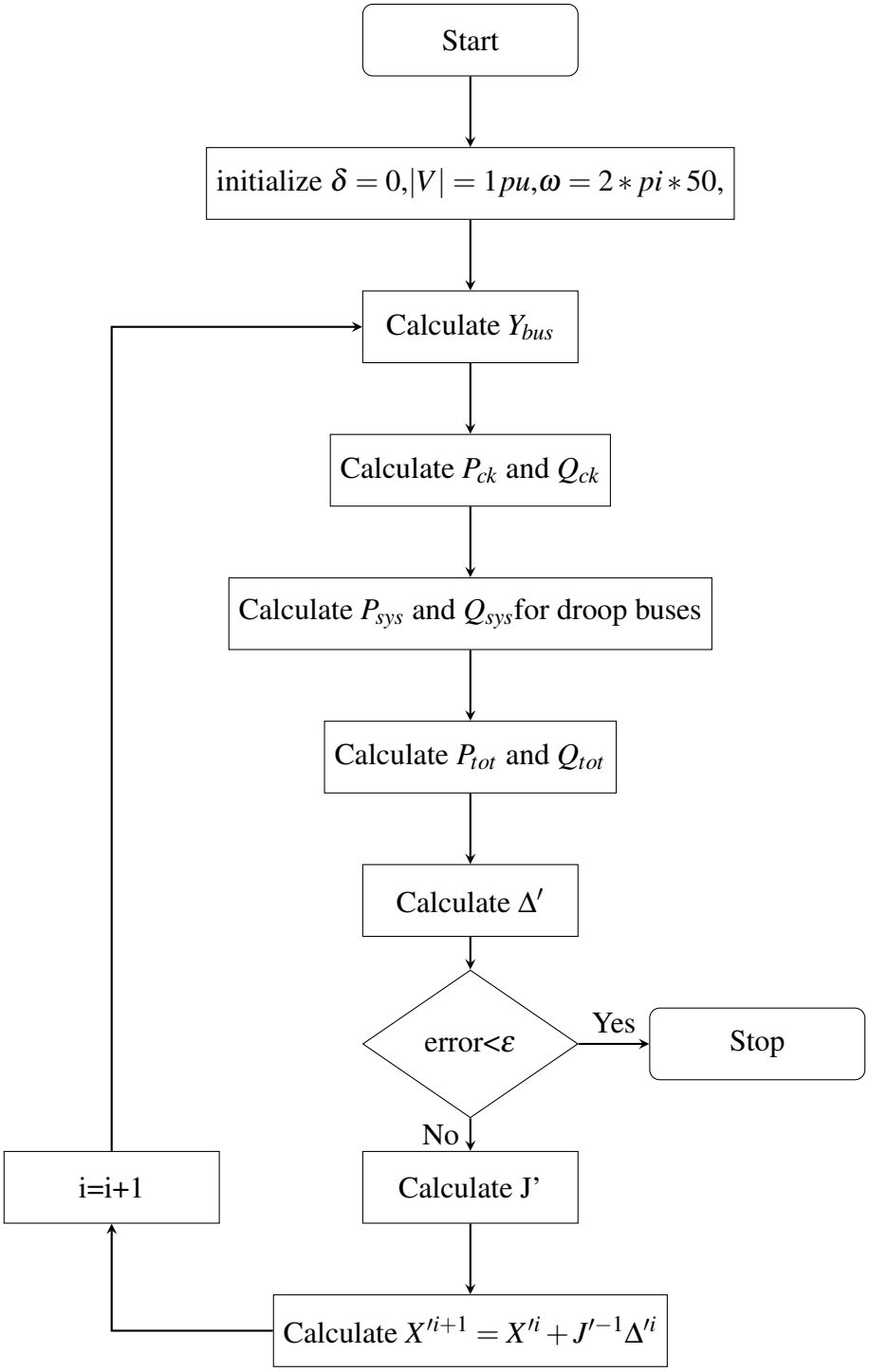

Figure 3.2: Flowchart of the MNR method

If not, the modified Jacobian is calculated using equation Eq 3.28 to be then multiplied with the mismatch vector, in order to find the difference to be added to the state vector (X').
Step11:

The number of iterations is increased by one and the algorithm uses the updated (X') to perform the next iterations.

3.5 Conclusion

In this chapter the detailed theory of the Modified Newton Raphson technique is presented. The MNR method holds an edge over the method presented in the previous chapter because of:

- First, Newton Raphson is used, which decreases the error quadratically, that is better than the Gausse seidal or the meta-heuristic methods(PSO and DE).
- Second,only one loop is used because the microgrid's equilibrium opearting points are found inside the MNR loop in step10.
- Third It can be coded in MATLAB, thus the debugging becomes easier which makes the algorithm more flexible.

In the next chapter the results of the MNR technique are shown and discussed.

Chapter 4

Simulation Results and discussion

4.1 Introduction

After explaining the method investigated in this thesis, in this chapter the load flow analysis using the Modified Newton Raphson technique is conducted on three microgrid benchmarks. The first being the 7-bus system which validated the algorithm present in [13]. The second is the 6-bus system which is a rather simple network with few transmission lines. The last is the 38-bus system which is the most challenging system due to its large number of buses and the weakly meshed topology.

4.2 Seven-bus System

4.2.1 Seven-bus microgrid analysis

To validate the proposed power flow approach, the previous method is applied to 0.4 kV islanded MG demonstrated on a 7-bus system shown in Fig 4.1 and simulated using MATLAB R2016a. The network consists of seven buses, two of them are load buses, one with constant power load(CP) and the other with a constant impedance (CZ) load and three DG units and two empty buses used for connection.

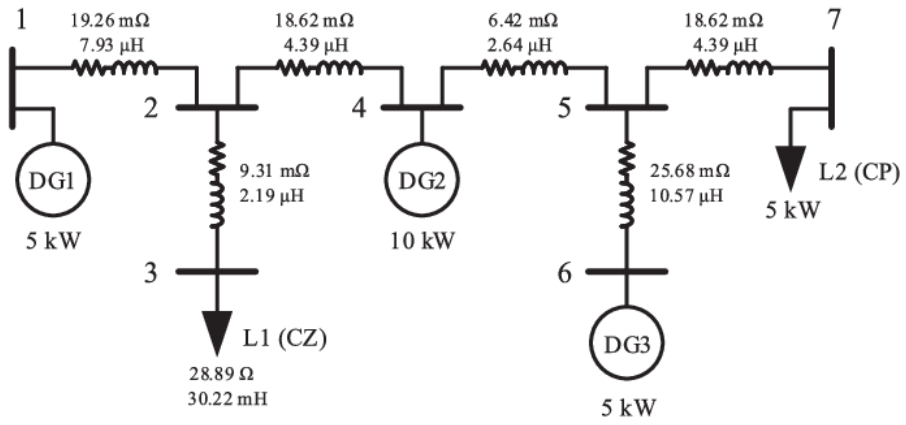

Figure 4.1: 7-bus system.

Table 4.2: Bus classification for the $7-bus$ system

Bus number	Bus type
1	Generation bus (Droop bus)
2	Load bus(zero load) (PQ)
3	Load bus (PQ)
4	Generation bus (Droop bus)
5	Slack bus
6	Generation bus(Droop bus)
7	Load bus (PQ)

- The well defined types of buses in the literature are slack, PV and PQ buses. The selection of bus depends upon the pre-specified quantities. In general, any bus can be a reference bus. In our circuit the slack bus is randomly selected on bus 5. For the DG's buses they are labelled as droop buses, as their known parameters are dependent on the droop equations. However since their known quantities are P_{inj} and Q_{inj} they are treated as PQ buses in the load flow code. Contrary to grid connected mode, where DG's are usually modeled as PV buses.
- The nominal power factor of the DG units is 0.85 while the loads operate with inductive power factor equal to 0.95.
- The entire network elements are operating at their nominal value and the time domain calculation are provided in [13].

Table 4.1: Initial conditions of the 7-bus system.

Power		$P_7(W)$	$P_i(W)$	$Q_7(VAR)$	$Qi(VAR)$	
Value		-5000	0	-4750	0	
		m(Hz/Kw)			n(V/KVAR)	
Droop coefficients	m_1	m_2	m_3	n_1	n_2	n_3
value	0.4	0.2	0.4	12.909	6.4543	12.909
Variable		ω	ω_{max}	V_i	V_{max}	
Value		$2*\pi*50$	$2*\pi*51$	400	400.06	

‘

4.2.2 Validation of the algorithm

```
Command Window
>> main_7bus_5_SB
************************ Results ********************************

-----------Voltages (V) ---------  Angles (degrees)-------------
bus_1      389.5660                -0.0108
bus_2      388.3076                0.0255
bus_3      387.1542                0.0678
bus_4      389.4198                -0.0141
bus_5      388.9702                0.0000
bus_6      390.6364                -0.0401
bus_7      386.5023                0.0903
*****************************************************************

------- Real Powers P(KW)-------- Reactive Powers Q(KVAR)----
DG_1       2.44032                      0.81254
DG_2       4.88064                      1.64777
DG_3       2.44032                      0.72961
*****************************************************************

----------------------Frequency(Hz) ----------------------------
                        50.0239  Hz
*****************************************************************
------- Excution time (s)------ iterations(overall number)--------
            0.1473                       18
*****************************************************************
---------------------- The Maximum Errors----------------------
Max_error_P = 0.0057 %
Max_error_Q = 0.0192 %
Max_error_V = 0.0027 %
```

Figure 4.2: The output of the 7-bus system.

The results of both the proposed algorithm and the time domain simulation done by Psim are shown bellow:

Network Bus Voltage(V)							
Bus	1	2	3	4	5	6	7
Psim	389.575	388.315	387.162	389.429	388.978	390.647	386.507
Proposed	389.566	388.307	387.154	389.419	388.970	390.636	386.502
Powers	P_{G1}	P_{G2}	P_{G3}	Q_{G1}	Q_{G2}	Q_{G3}	
Psim	2.44046	4.88086	2.44042	0.81238	1.64756	0.72951	
Proposed	2.44032	4.88064	2.44032	0.81254	1.64777	0.72961	
Maximum error							
	Max error of P	Max error of Q	Max error of V	Max error of F			
	0.0057%	0.0192 %	0.0027%	$2*10^{-4}$%			

Table 4.3: Results comparison.

- Time domain (TD) simulations in [13] are performed using PSIM software. All their simulations are performed using an Intel Core i7-930, 2.8 GHz, RAM 24 GB, personal computer. Our algorithm is validated using Intel(R) Core(TM) i5-8350U CPU @ 1.70GHz 1.90 GHz, RAM 8 GB,personal computer.
- The execution time using MATLAB was 0.1473 seconds which is small compared to that of the paper [13] in which their algorithm converges in 2.065 seconds. This difference is due to the fact that we only used MATLAB to run the algorithm with no other softwares.
- The overall number of iterations is reduced to only 18 iterations. When the algorithm of [13] was tested the outer loop number of iterations was 16 but the overall number reaches 139 iterations. This is because, unlike the MNR technique, which updates the frequency and slack bus voltage inside the load flow analysis function, conventional LFA is conducted in [13] before the frequency and slack bus voltage are updated.
- Not only the number of iteration was reduced, but our results are even more similar to the PSIM results than the suggested algorithm in[13] as shown in 4.10.
- The sole negative is that the Jacobian matrix used in this case has grown from 12 by 12 to 14 by 14, which requires additional computing time.

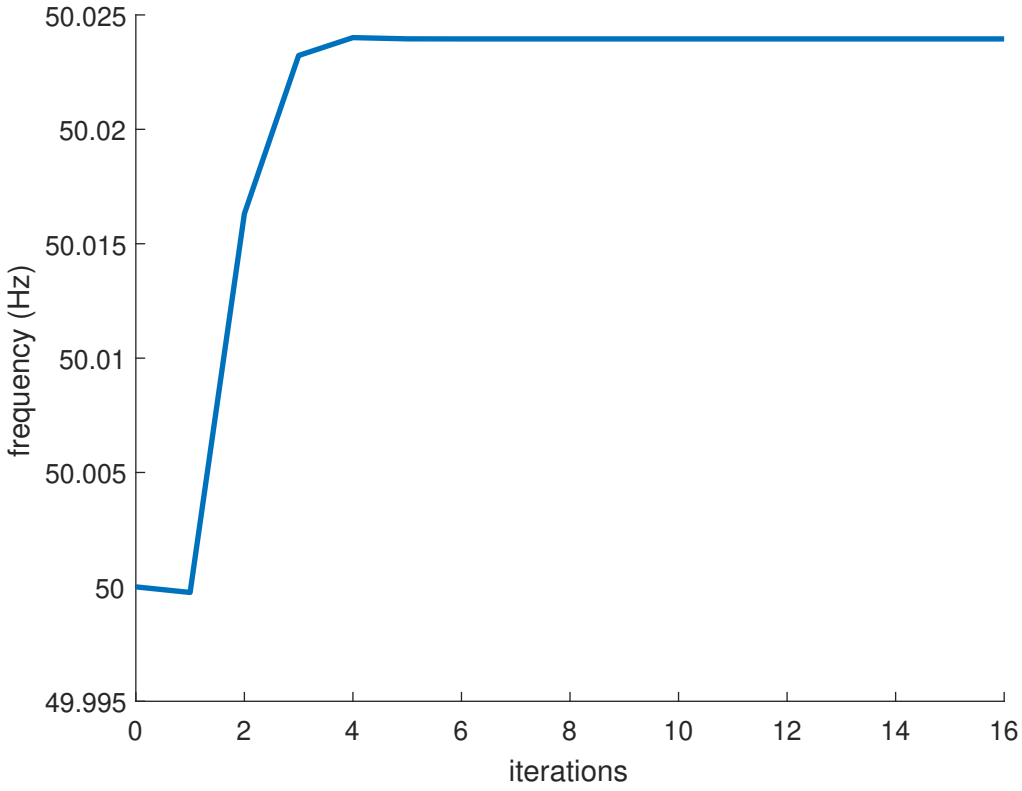

Figure 4.3: Frequency variation each iteration.

The results shown in table 4.3 are demonstrated in the bar plots below in Fig 4.7, 4.8, 4.9 and the difference between the reference results and the proposed ones is negligible and it cannot be seen.

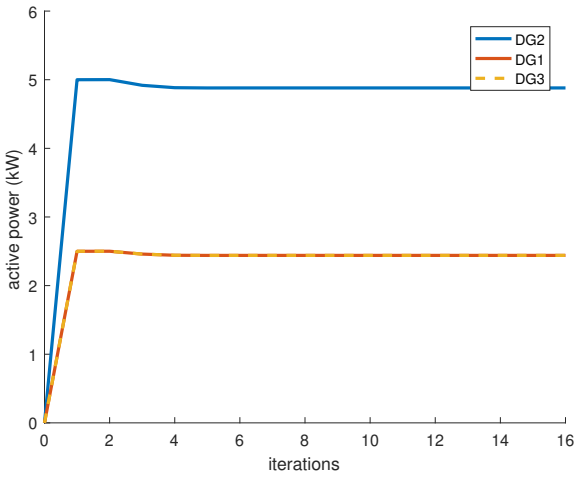

Figure 4.4: Active power with respect to iterations.

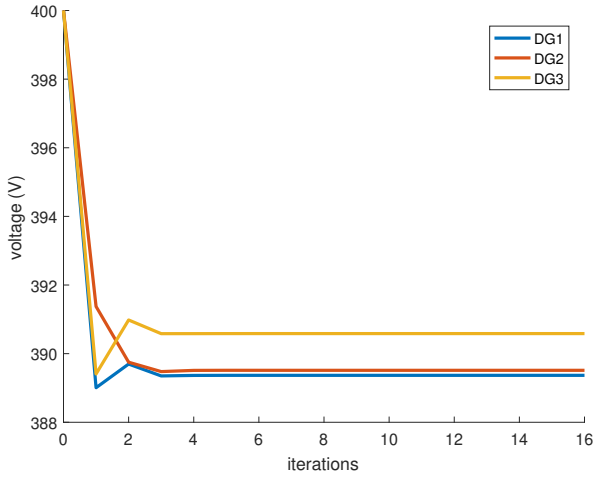

Figure 4.5: Voltage levels each iteration.

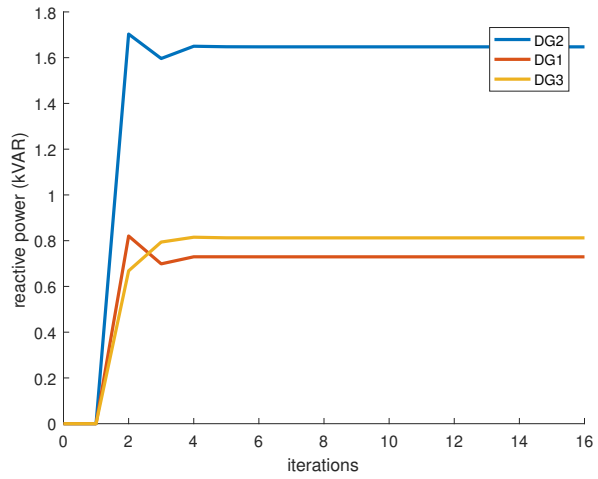

Figure 4.6: Reactive Power variation each iteration.

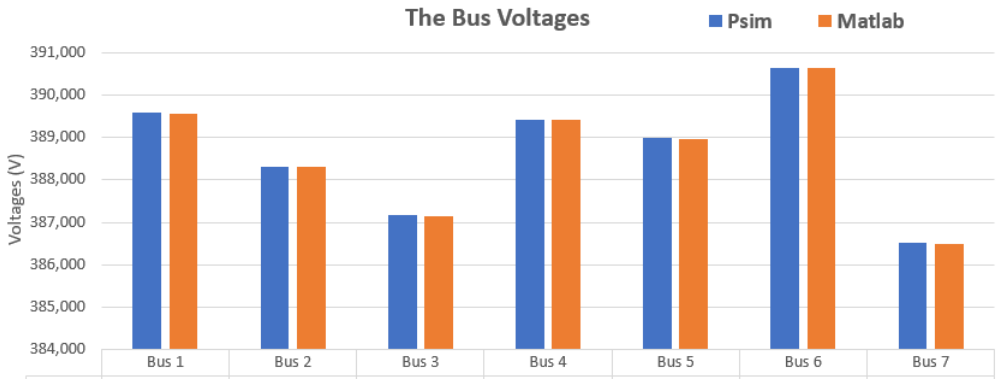

Figure 4.7: Voltage level comparison.

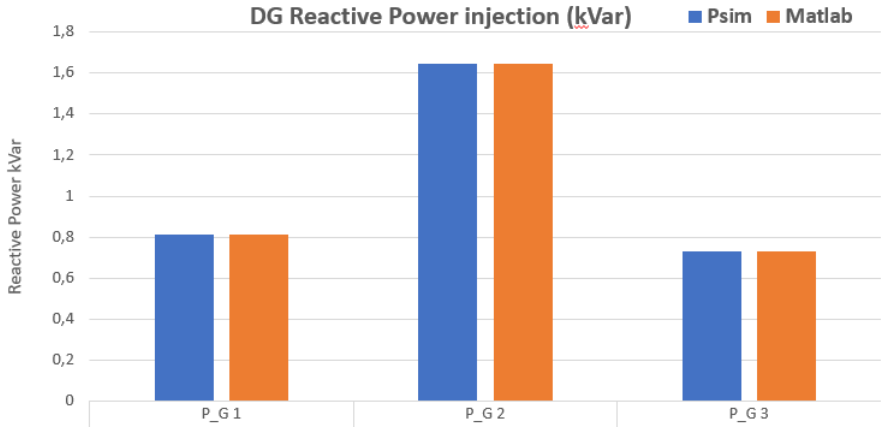

Figure 4.8: Reactive power results comparison.

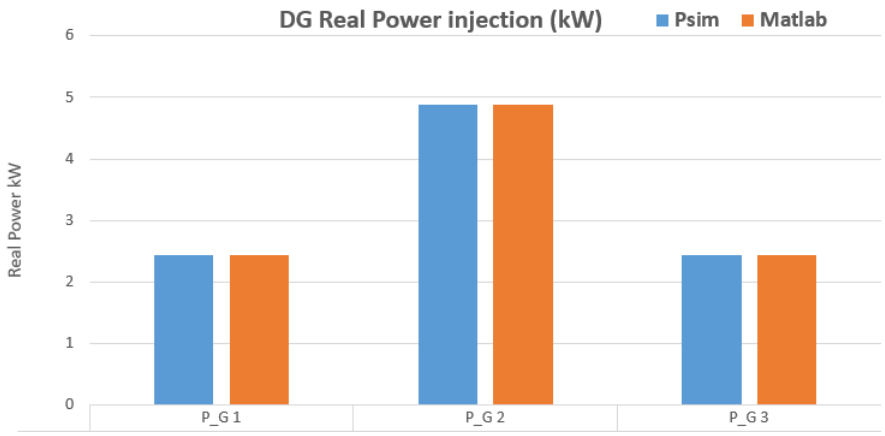

Figure 4.9: Active power results comparison.

It can be seen that the active power generation is the same in the DG's with the same nominal value, this is due to the fact that all the DG's operates at the same frequency. However there is a small difference between the reactive power generation and this is due to the difference in the voltage level at the generation bus. The voltage level is at its highest in the generation buses and at its lowest in the load buses because the DG's are injecting reactive power not absorbing.

4.2.3 Results comparison with other methods

AS discussed in chapter 2 many methods are developed to solve the LFA for microgrid. Two algorithms which the flowcharts are given in Figs 2.2 and 2.3 were coded in Matlab in [9] to solve the 7-bus system. The results obtained from the two algorithms and the MNR algorithm are presented in the radar plot in Fig 4.10 below :

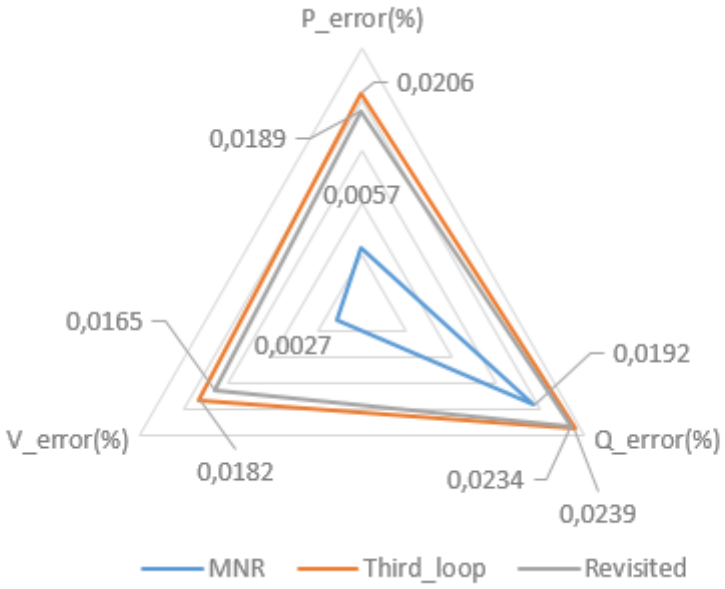

Figure 4.10: Radar plot for error comparison.

The values of active power, reactive power and the voltage of each of the three algorithms are compared with the ones from the PSIM simulation of the 7-bus system given in [1].

The plot presents all the errors one in each corner and all of the three methods each one with a different color. The closer to the center the plot is, the better the results are.

This plot allowed us to see that the two other algorithm are arguably similar. However the MNR technique has slightly better results regarding the reactive power error, but it has a significantly smaller error in both the active power and the voltage magnitude.

4.2.4 Changing the slack bus position

In the test the slack bus position is changed from bus-5 to bus-1. The first being an empty bus with no generated or consumed power and the second is a power generation bus. The results are shown in fig 4.11.

As it can be seen neither the voltage magnitude nor the the power generated has changed when the slack bus position was changed. However the angles have changed as expected since the reference angle was changed from bus-5(it was zero earlier) to bus-1.

This shows that the slack bus is only used as a reference, unlike in the CLF where it has to be large enough to compensate the system losses. This confirms the claim that the the slack bus can be chosen randomly to be at any bus.

```
Command Window
>> main_7bus
************************ Results ********************************

-----------Voltages (V) ---------  Angles (degrees)------------
bus_1      389.5660                0.0000
bus_2      388.3076                0.0362
bus_3      387.1542                0.0786
bus_4      389.4198                -0.0034
bus_5      388.9702                0.0108
bus_6      390.6364                -0.0293
bus_7      386.5023                0.1011
*****************************************************************

------- Real Powers P(KW)-------- Reactive Powers Q(KVAR)----
DG_1      2.44032                      0.81254
DG_2      4.88064                      1.64777
DG_3      2.44032                      0.72961
*****************************************************************

---------------------Frequency(Hz) ---------------------------
                      50.0239  Hz
*****************************************************************
------- Excution time (s)------ iterations(overall number)--------
            0.0832                       18
*****************************************************************
---------------------- The Maximum Errors----------------------
Max_error_P = 0.0057 %
Max_error_Q = 0.0192 %
Max_error_V = 0.0027 %
```

Figure 4.11: Bus-1 taken as slack bus in the 7-bus system.

4.3 Six bus system

To further validate the algorithm, a 6-bus system is used to test it. The system is constructed three load buses and three DG's buses in addition to five transmission lines as shown in 4.12.

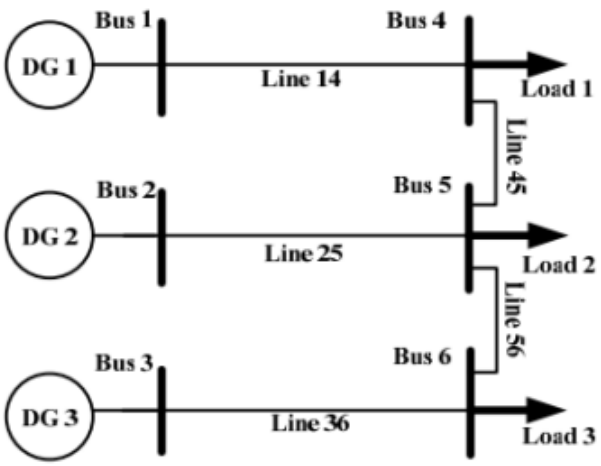

Figure 4.12: 6-bus test system.

4.3.1 Six bus Microgrid analysis

The data of the loads, transmission lines and the coefficients of the distributed generators found in [14] are presented in the table 4.4. In addition to the initial conditions used in the code.

Table 4.4: 6-bus system parameters.

Parameters	Symbol	Value	Units
Power stage			
Line resistance	R(i,j)	0.15	Ω
Line inductance	L(i,j)	0.062	mH
LC filter inductor	$L_{DG}(i)$	1.8	mH
LC filter capacitor	$L_{DG}(i)$	2.7	µF
Load parameters			
Bus number	$R_{load}(\Omega)$	$L_{load}(H)$	
Bus 4	90	0.0609	
Bus 5	110	0.0836	
Bus 6	100	0.25136	
Control parameters			
Distributed generator	m(rad/W*s)	n(V/VAR)	
DG 1	0.001	0.02	
DG 2	0.0005	0.01	
DG 3	0.004	0.02	
Initial values			
Distributed generator	V_i	P_G	$Q_G(VAR)$
DG1	220	0	152.5
DG2	220	0	305
DG3	220	0	152.5
Variables	Value		
ω_{max}	$2*\pi*51$		
ω	$2*\pi*51$		
V_{max}	226.1		

4.3.2 Validation of the Six-bus system

- As can be seen the nominal active and reactive power of the DG's were not provided in the data presented, as well as the resulting active and reactive power. In the other hand we are given the constant load impedance, the droop coefficients and the nominal voltage level in the data. In addition to the output voltage in the results of [14] which is enough to calculate the consumed and the generated power. Here we validated the algorithm based on the voltage level shown in Fig 4.13.
- The buses of the the six-bus system are either generation bus or a load bus, thus the load bus are taken as (PQ) buses and the generation bus are taken as droop buses except bus1 which is taken as the slack bus. As shown in Fig 4.5 below.

The proposed algorithm in Fig 3.2 is developed in MATLAB using the data from Fig 4.4 and tested on the system in Fig 4.12, the results are as follows:

Table 4.5: Bus classification for the 6-bus system.

Bus number	Bus type
1	Slack bus
2	Generation bus (Droop bus)
3	Generation bus (Droop bus)
4	Load bus (PQ)
5	Load bus (PQ)
6	Load bus (PQ)

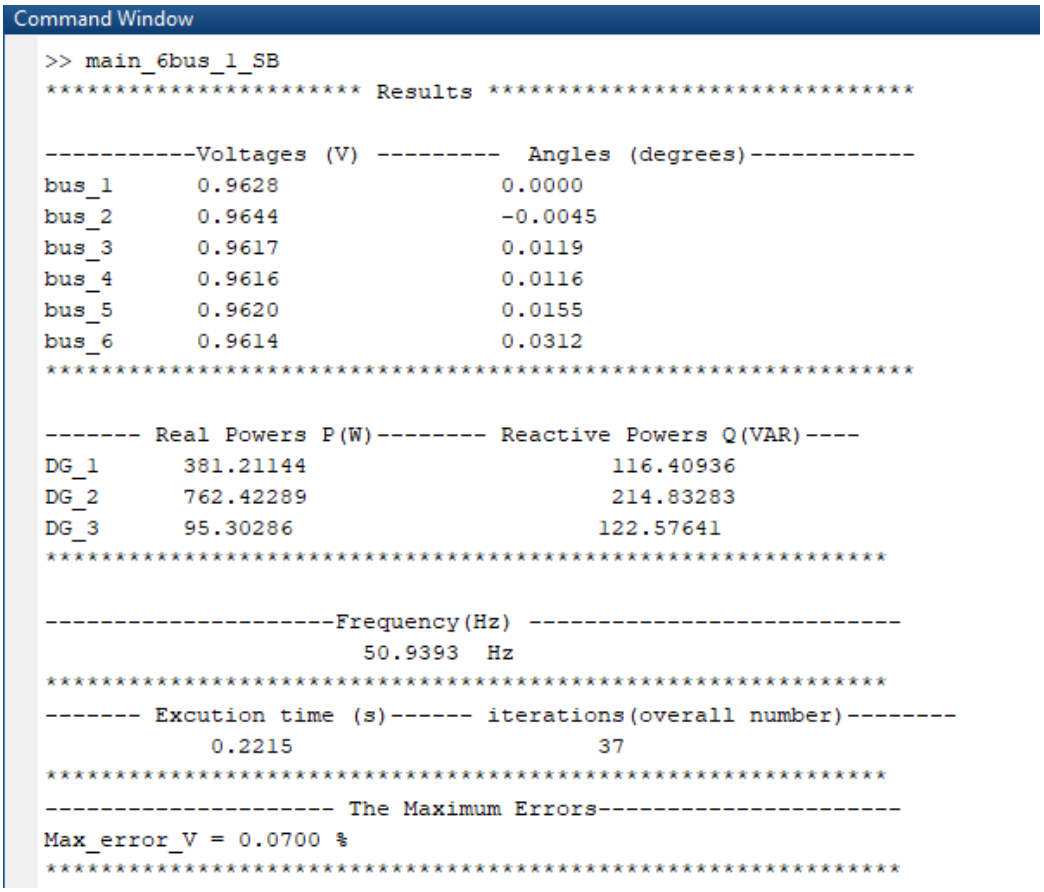

Figure 4.13: The output of the 6-bus system.

Network Bus Voltage(pu)						
Bus	1	2	3	4	5	6
Psim	0.9629	0.9645	0.9624	0.9618	0.9623	0.9619
Proposed	0.9628	0.9644	0.9617	0.9616	0.9620	0.9614
Maximum error						
Bus	1	2	3	4	5	6
voltage error	0.0106 %	0.0143 %	0.0700%	0.0176%	0.0273%	0.0211%

Table 4.6: Results comparison.

- As observed in the table, the maximum error between the voltage calculated and that of the simulation results obtained from [14] is about 0.070% which is even smaller than the smallest error found in [14]. This accordance in results shows the accuracy of the MNR method in solving LV microgrids in islanded mode with droop control DG's.
- The following graphs represents the active power, the voltage level and the reactive power of the DG buses in addition to the frequency.
- As can be seen in Fig 4.14 and Fig 4.16 the active power is inversely proportional to the frequency because of the droop characteristics. Furthermore the active power and the frequency converge around the second iterations, due to the inclusion of the frequency in the state vector X'.
- In the graphs of the voltage and the reactive power Fig 4.17 and Fig 4.16 respectively. It can be seen that they are taking longer time to converge compared to the frequency and the active power, because the frequency is updated using only $P_{sys} - P_{tot}$, whereas the voltage is related to the Q_{DG} and Q_{ck} leading to more complicated calculations which means more computational time.

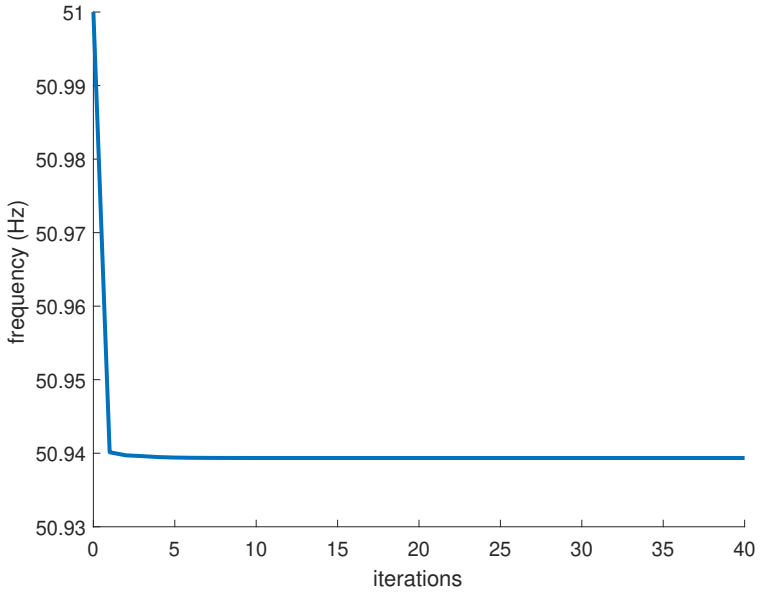

Figure 4.14: Frequency with respect to iteration.

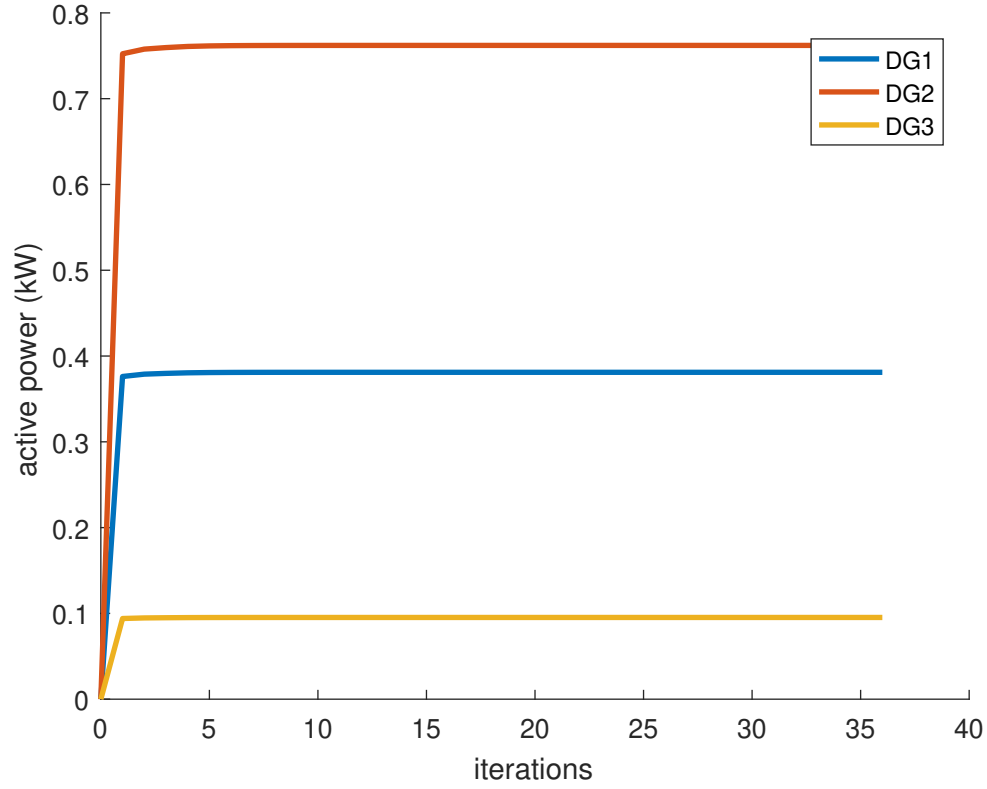

Figure 4.15: Active power each iteration.

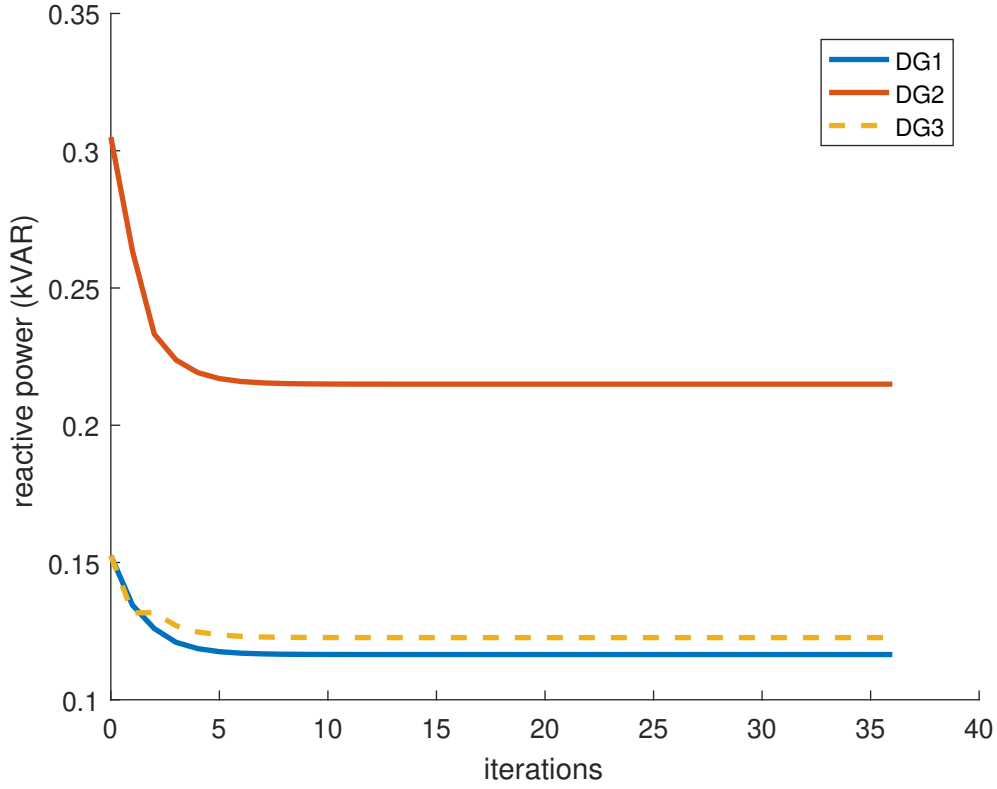

Figure 4.16: Reactive power with respect to iterations.

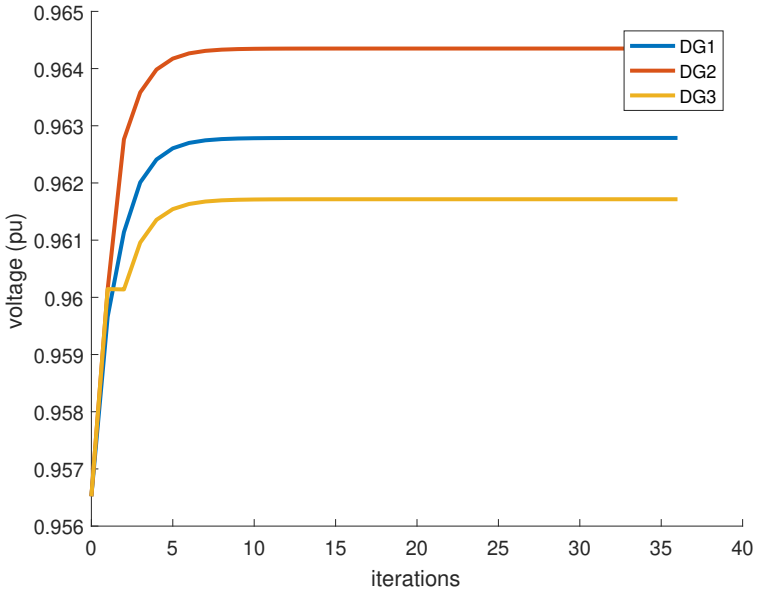

Figure 4.17: Voltage level with respect to iteration.

The output voltages of the the proposed algorithm and the results of the PSIM simulation in addition to the results from [14] are shown in the bar plot below:

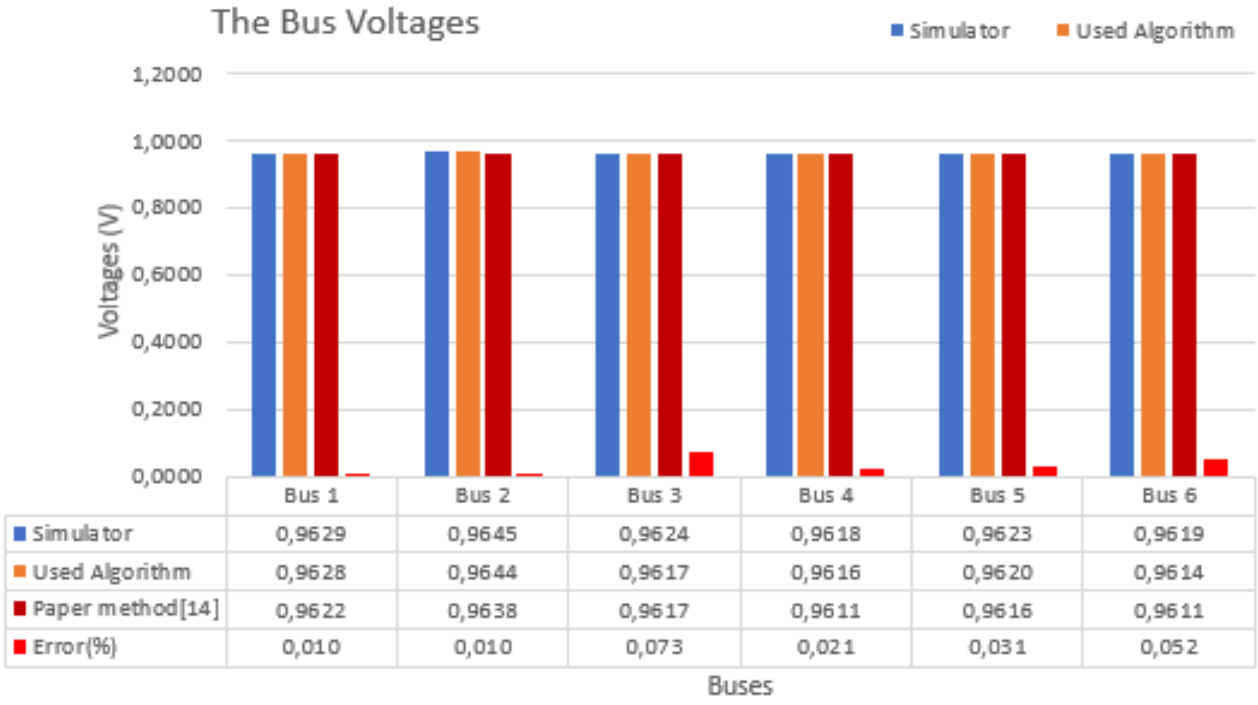

	Bus 1	Bus 2	Bus 3	Bus 4	Bus 5	Bus 6
Simulator	0,9629	0,9645	0,9624	0,9618	0,9623	0,9619
Used Algorithm	0,9628	0,9644	0,9617	0,9616	0,9620	0,9614
Paper method[14]	0,9622	0,9638	0,9617	0,9611	0,9616	0,9611
Error(%)	0,010	0,010	0,073	0,021	0,031	0,052

Figure 4.18: Bar plots for voltage magnitudes and errors.

As can be seen the results of the proposed algorithm are the closest to the PSIM simulation with a significantly small error.

4.3.3 Changing the slack bus position

This test is performed as well on the 6-bus system, where the slack bus is changed from bus-1 to bus-2(notice the angle is 0°). As shown in the Fig 4.19 the output voltage has not changed at all as the errors stayed same, but as expected we notice a variation in the angles as the reference changed . This Modified Newton Raphson technique is not affected by the slack bus position. This later can be taken at any bus, chosen randomly and the results gotten are exactly the same. As confirmed in the figures Fig 4.19 and Fig 4.11, where the slack bus is chosen to be bus-2 and the results are not changed. This gives the technique more flexibility unlike in the conventional grid where the slack bus needs to be powerful enough to compensate the system losses.

```
Command Window
>> main_6bus_2_SB
************************ Results ********************************

-----------Voltages (V) ---------  Angles (degrees)------------
bus_1      0.9628                0.0045
bus_2      0.9644                0.0000
bus_3      0.9617                0.0164
bus_4      0.9616                0.0161
bus_5      0.9620                0.0200
bus_6      0.9614                0.0357
*****************************************************************

------- Real Powers P(W)-------- Reactive Powers Q(VAR)----
DG_1      381.21144                     116.40936
DG_2      762.42289                     214.83283
DG_3      95.30286                     122.57641
*****************************************************************

---------------------Frequency(Hz) ----------------------------
                      50.9393  Hz
*****************************************************************
------- Excution time (s)------ iterations(overall number)--------
            0.2703                     37
*****************************************************************
---------------------- The Maximum Errors----------------------
Max_error_V = 0.0700 %
*****************************************************************
```

Figure 4.19: Bus-2 taken as slack bus in the 6-bus system.

4.4 38-Bus System

The algorithm is to be tested on a bigger scale system with larger number of buses. The system consists of five DG's and 32 loads with only 37 transmission lines. The system buses are connected radially this makes the system weakly meshed which means there is a limited number of interconnection between the busses. Radial networks can show a severe voltage drop from a bus to the next one and also they limit the network's ability to share the load between the distributed generators.

4.4.1 38-bus Microgrid Analysis

The following diagram shown in Fig 4.20 is a representation of the 38-bus system, it consists of one empty bus taken as slack, 32 load buses taken as PQ buses and 5 DG's modelled as droop buses. The droop coefficients of the DG's as well as the maximum value of the voltage ans frequency are shown in table 4.7.

The active and reactive power consumed by each load in addition to the transmission lines impedances are taken from [15].

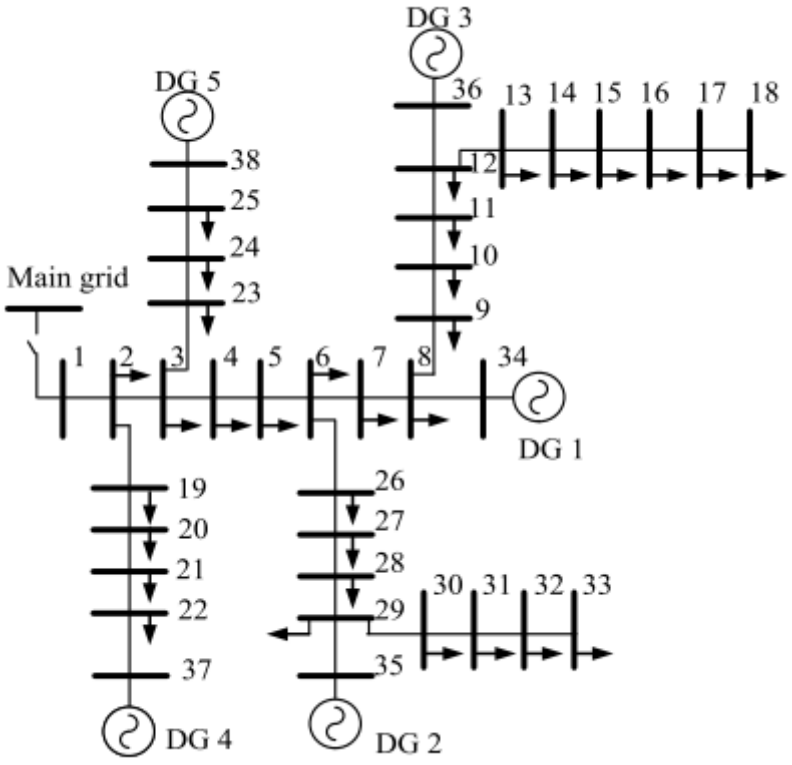

Figure 4.20: 38-bus system topology.

Table 4.7: Distributed generators data of the 38-bus system.

Node	m_p	n_q	ω_{max}	V_{max}	Q_{DGmax}	P_{DGmax}
34	0.005102	0.02	1	1.01	0.9	0.5
35	0.001502	1/30	1	1.01	0.6	1.5
36	0.004506	0.02	1	1.01	0.9	0.5
37	0.002253	0.135	1	1.01	1/9	0.9
38	0.002253	0.05	1	1.01	0.3	0.9

All the values are in pu

4.4.2 Validation of the Algorithm on the 38 bus

Using the data mentioned above the system is simulated in Matlab, the MNR is then performed on the 38-bus. The bus classification is as follows:

Table 4.8: Bus classification.

Bus	Type
1	Slack bus
2...33	PQ buses
34...38	Droop buses

The results obtained from the algorithm of the voltages, active power and reactive power are shown in the two Fig 4.21 and 4.22.

Command Window

```
>> main_38
************************ Results ********************************

-----------Voltages (V) --------- -- Angles (degrees)-----------
----Our results------Reference----Reference----Our results
bus_1   0.9400        0.9403        0.0000        0.0000
bus_2   0.9400        0.9403        0.0000       -0.0000
bus_3   0.9417        0.9420        0.0106        0.0104
bus_4   0.9434        0.9437        0.0131        0.0126
bus_5   0.9455        0.9458        0.0142        0.0134
bus_6   0.9511        0.9514        0.1023        0.1006
bus_7   0.9577        0.9580        0.4214        0.4218
bus_8   0.9682        0.9685        0.2527        0.2533
bus_9   0.9818        0.9819        0.5600        0.5609
bus_10  0.9867        0.9869        0.6408        0.6445
bus_11  0.9884        0.9878        0.6397        0.7847
bus_12  0.9903        0.9896        0.6358        0.7813
bus_13  0.9924        0.9917        0.8776        1.0239
bus_14  0.9932        0.9925        1.0123        1.1591
bus_15  0.9950        0.9943        1.1270        1.2741
bus_16  0.9976        0.9969        1.2571        1.4045
bus_17  1.0027        1.0019        1.6744        1.8230
bus_18  1.0060        1.0052        1.8219        1.9708
bus_19  0.9395        0.9398       -0.0135       -0.0135
bus_20  0.9361        0.9364       -0.0988       -0.0989
bus_21  0.9355        0.9358       -0.1230       -0.1230
bus_22  0.9349        0.9352       -0.1465       -0.1465
bus_23  0.9414        0.9417        0.0191        0.0192
bus_24  0.9416        0.9418        0.0432        0.0441
bus_25  0.9447        0.9450        0.1160        0.1178
bus_26  0.9495        0.9498        0.1268        0.1248
```

Figure 4.21: Results of the 38-bus system.

As expected the voltage magnitudes is decreasing from a bus to another. The buses closest to the DG's have a higher voltage magnitude. The results of [16] are used as reference to compare and test the accuracy of results. The results of our algorithm are in accordance with those of the reference we can see in the Fig 4.23 that voltage difference is so small in all the busses except for the 31,32 and 33 buses which are the furthest from the DG's and have the smallest values in both results.

From the bar plot of the voltage magnitude shown in Fig 4.23, we can see the voltage drop more clearly as well as the comparison between the results.

From the bar plots of the active and reactive power in Fig 4.25 and Fig 4.24 we notice that the results are almost identical and the difference is negligible which shows the robustness and the flexibility of the MNR algorithm which serve as a great tool to solve such weakly meshed system.

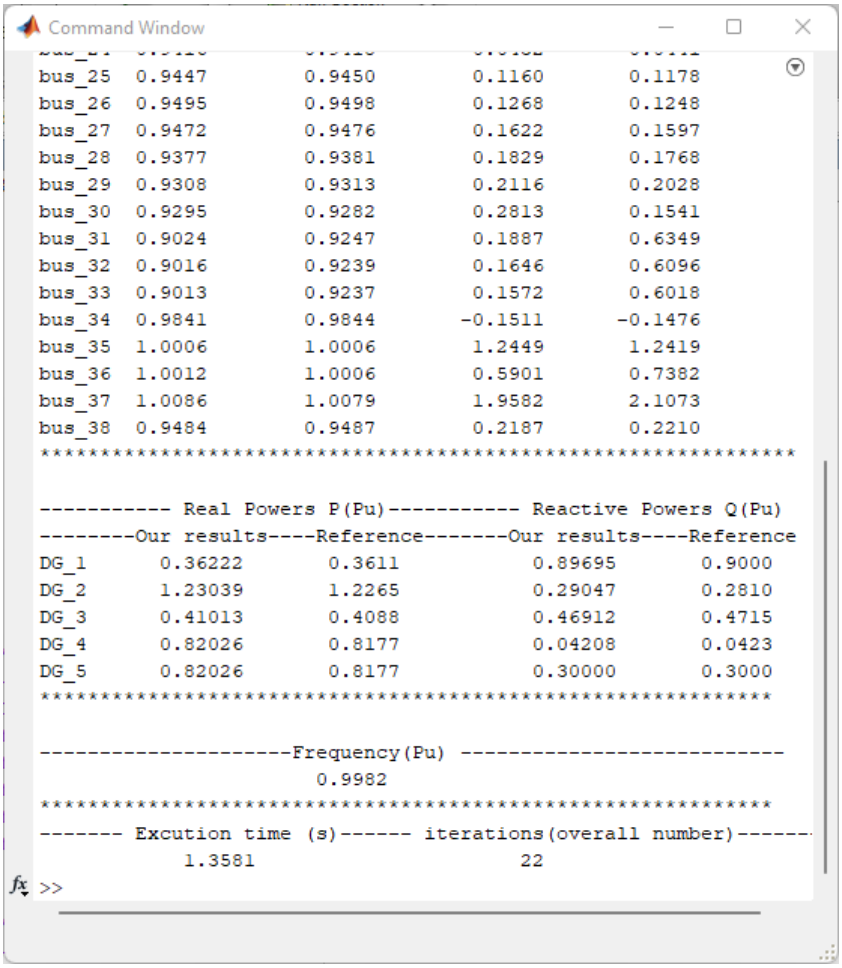

Figure 4.22: Results of the 38-bus system(second part).

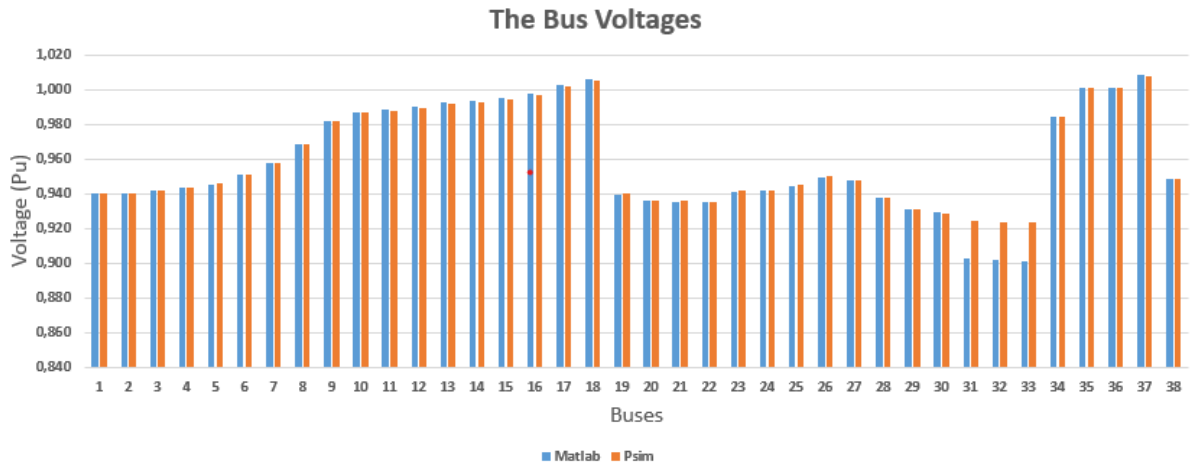

Figure 4.23: Voltage level at each bus.

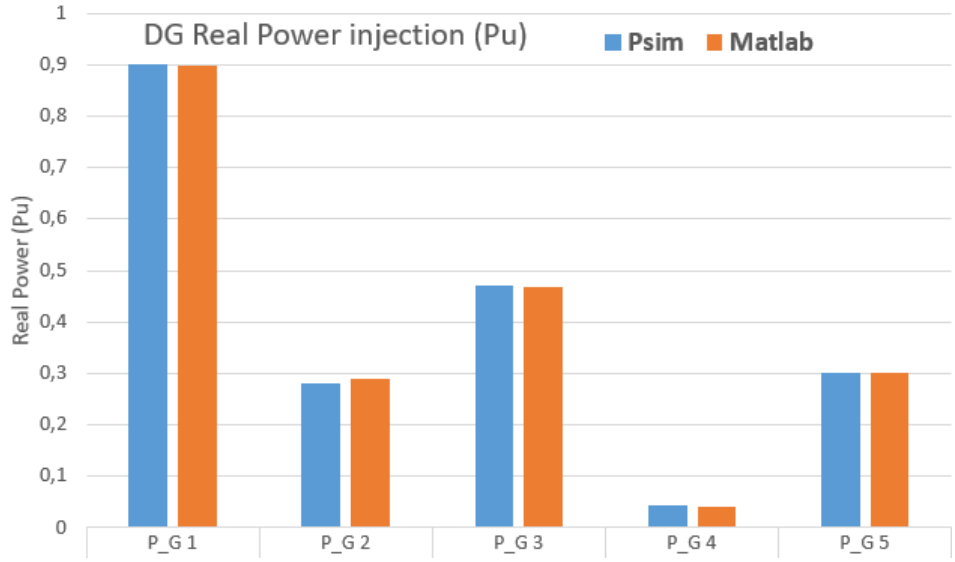

Figure 4.24: Active power comparison at each of the DG buses.

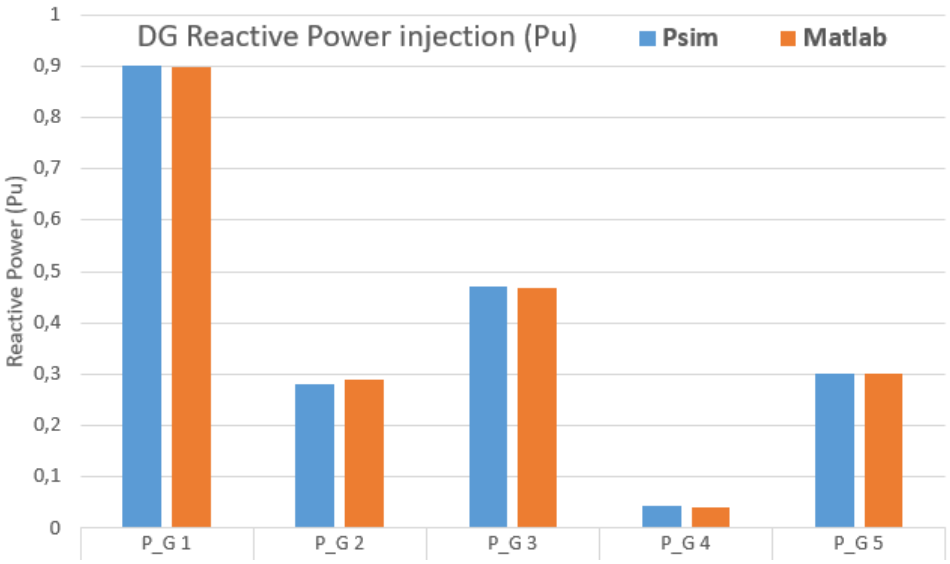

Figure 4.25: Reactive power comparison at each of the DG buses.

4.4.3 Changing the slack bus position

This test is once again performed on the 38-bus system. The slack is changed from bus-1 which is a en empty bus with no generated or consumed power, to bus-38 a generation bus labeled as DG_5. The reference has changed to bus-38 as its angle is zero and all the other angle has shifted with respect to that. Neither the power generated nor the voltage level have changed except for the number of iteration that increased slightly.

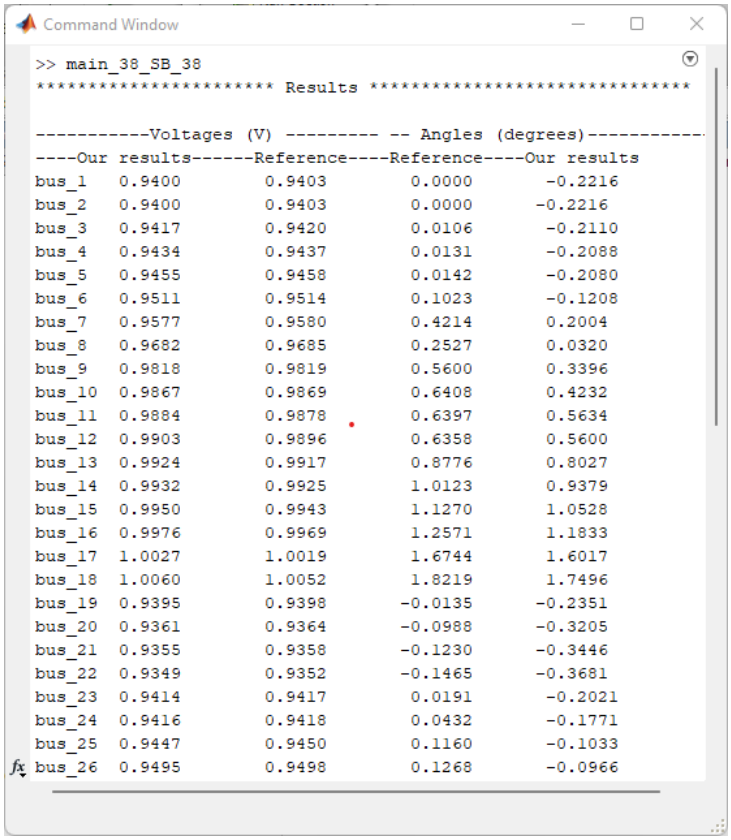

```
Command Window
>> main_38_SB_38
********************** Results ********************************

-----------Voltages (V) --------- -- Angles (degrees)-----------
----Our results------Reference----Reference----Our results
bus_1   0.9400        0.9403        0.0000       -0.2216
bus_2   0.9400        0.9403        0.0000      -0.2216
bus_3   0.9417        0.9420        0.0106       -0.2110
bus_4   0.9434        0.9437        0.0131       -0.2088
bus_5   0.9455        0.9458        0.0142       -0.2080
bus_6   0.9511        0.9514        0.1023       -0.1208
bus_7   0.9577        0.9580        0.4214        0.2004
bus_8   0.9682        0.9685        0.2527        0.0320
bus_9   0.9818        0.9819        0.5600        0.3396
bus_10  0.9867        0.9869        0.6408        0.4232
bus_11  0.9884        0.9878        0.6397        0.5634
bus_12  0.9903        0.9896        0.6358        0.5600
bus_13  0.9924        0.9917        0.8776        0.8027
bus_14  0.9932        0.9925        1.0123        0.9379
bus_15  0.9950        0.9943        1.1270        1.0528
bus_16  0.9976        0.9969        1.2571        1.1833
bus_17  1.0027        1.0019        1.6744        1.6017
bus_18  1.0060        1.0052        1.8219        1.7496
bus_19  0.9395        0.9398       -0.0135       -0.2351
bus_20  0.9361        0.9364       -0.0988       -0.3205
bus_21  0.9355        0.9358       -0.1230       -0.3446
bus_22  0.9349        0.9352       -0.1465       -0.3681
bus_23  0.9414        0.9417        0.0191       -0.2021
bus_24  0.9416        0.9418        0.0432       -0.1771
bus_25  0.9447        0.9450        0.1160       -0.1033
bus_26  0.9495        0.9498        0.1268       -0.0966
```

Figure 4.26: 38-bus results as the bus-38 is the slack bus.

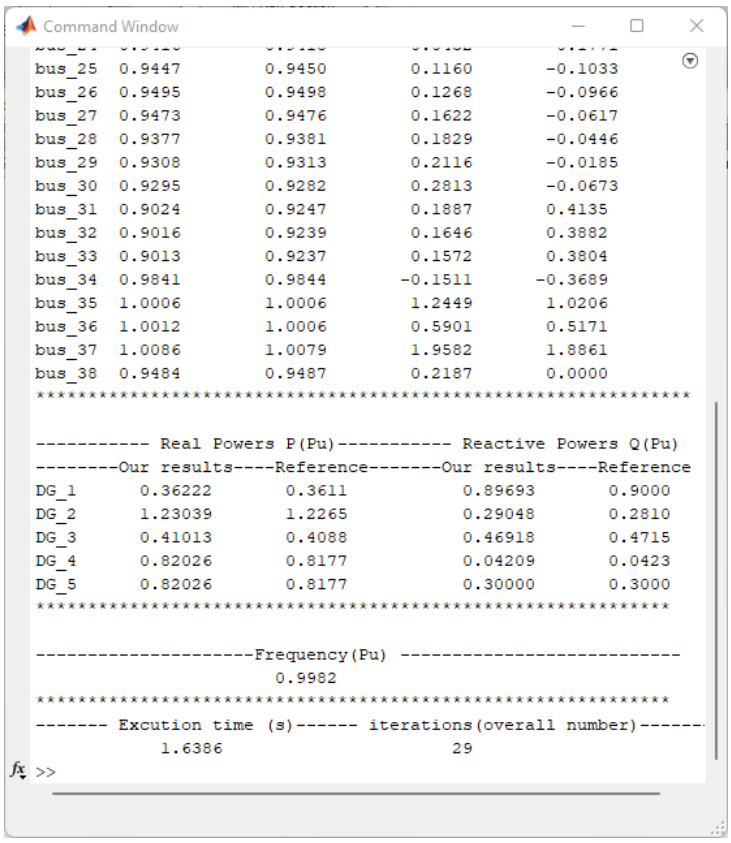

```
Command Window
bus_25  0.9447        0.9450        0.1160       -0.1033
bus_26  0.9495        0.9498        0.1268       -0.0966
bus_27  0.9473        0.9476        0.1622       -0.0617
bus_28  0.9377        0.9381        0.1829       -0.0446
bus_29  0.9308        0.9313        0.2116       -0.0185
bus_30  0.9295        0.9282        0.2813       -0.0673
bus_31  0.9024        0.9247        0.1887        0.4135
bus_32  0.9016        0.9239        0.1646        0.3882
bus_33  0.9013        0.9237        0.1572        0.3804
bus_34  0.9841        0.9844       -0.1511       -0.3689
bus_35  1.0006        1.0006        1.2449        1.0206
bus_36  1.0012        1.0006        0.5901        0.5171
bus_37  1.0086        1.0079        1.9582        1.8861
bus_38  0.9484        0.9487        0.2187        0.0000
************************************************************

----------- Real Powers P(Pu)----------- Reactive Powers Q(Pu)
--------Our results----Reference-------Our results----Reference
DG_1      0.36222       0.3611           0.89693       0.9000
DG_2      1.23039       1.2265           0.29048       0.2810
DG_3      0.41013       0.4088           0.46918       0.4715
DG_4      0.82026       0.8177           0.04209       0.0423
DG_5      0.82026       0.8177           0.30000       0.3000
************************************************************

---------------------Frequency(Pu) ---------------------------
                      0.9982
************************************************************
------- Excution time (s)------ iterations(overall number)------
           1.6386                      29
>>
```

Figure 4.27: 38-bus results with bus-38 taken as slack bus.

4.5 Conclusion

In this chapter the algorithm is tested and our study is concluded, the results are presented and discussed. We have seen that the MNR technique provided the most accurate results with fewer iterations compared to other algorithms mentioned. In addition to ability to converge even in radial networks the MNR technique is independent of the slack bus position. This confirms that the MNR is indeed a useful tool regarding the LFA for islanded microgrid.

General Conclusion

Due to microgrid's unique behaviors during autonomous operation, it makes the design process more challenging especially power flow studies, therefore a new approach needs to be applied in order to solve the power flow problem.

This research has presented a powerful tool to address the challenges mentioned above. The main contribution of this thesis is summarized below.

A new load flow solution with the droop control characteristics is presented for islanded microgrid. The solution was based on extending the number of variables and equations of the conventional Newton Raphson. The main advantage of this method is the ability to give accurate enough results compared to the time domain simulation softwares in a significantly shorter time. The second advantage is the number of iterations where the load flow is performed has decreased significantly, due to the fact that the update of all the variables is done using the Newton Raphson technique which reduces the error quadraticaly. The algorithm was tested on a 7-bus, 6-bus and a 38-bus system, MATLAB is used to simulate the networks and the results obtained are compared with the time domain simulation done using PSIM. In all cases the algorithm's output was accurate enough even when tested on the larger weakly meshed 38-bus system. These results show the robustness and the accuracy of the algorithm in addition to its ability to solve different microgrid benchmarks. Therefore the algorithm is validated as a powerful tool for solving power flow problems in islanded microgrid.

After the validation of the Modified Newton Raphson technique the following future works can be conducted:

- Improving the MNR algorithm by adding the slack bus active and reactive power to the mismatch vector.
- Adding an acceleration factor to make the algorithm even faster.

References

[1] E. O. Kontis, G. C. Kryonidis, A. I. Nousdilis, K.-N. D. Malamaki, and G. K. Papagiannis, "Power flow analysis of islanded ac microgrids," in *2019 IEEE Milan PowerTech, Milan, Italy*, 2019, pp. 1–6. DOI: 10.1109/PTC.2019.8810612.

[2] N. Patel, D. Porwal, A. K. Bhoi, D. P. Kothari, and A. Kalam, "An overview on structural advancements in conventional power system with renewable energy integration and role of smart grids in future power corridors," in *Advances in Greener Energy Technologies*, A. K. Bhoi, K. S. Sherpa, A. Kalam, and G.-S. Chae, Eds. Singapore: Springer Singapore, 2020, pp. 1–15, ISBN: 978-981-15-4246-6. DOI: 10.1007/978-981-15-4246-6_1. [Online]. Available: https://doi.org/10.1007/978-981-15-4246-6_1.

[3] M.Paul, J.Miller, S.Knudsen, and T.Grabowski, "Electric power system asset optimization," *National Energy Technology Laboratory*, Mar. 2011. [Online]. Available: https://netl.doe.gov/sites/default/files/Smartgrid/ElecAssetOptRep.pdf.

[4] "The spectrum of resiliency – what role does energy storage play in a microgrid?" (Apr. 2018), [Online]. Available: https://microgridknowledge.com/energy-storage-microgrid/.

[5] M.Paul, J.Miller, S.Knudsen, and T.Grabowski, "Flywheel energy storage systems for ride-through applications in a facility microgrid '," *IEEE Transactions on Smart Grid*, 2011. DOI: 10.1109/TSG.2012.2212468.

[6] P. Yogita and M. Shweta Mishra, "''review on development of microgrid with renewable energy sources," *International Journal of Engineering Development and Research*, 2008.

[7] T. SON, "Islanding detection and power quality analysis in microgrid," Ph.D. dissertation, Shibaura Institute Of Technology, 2019.

[8] F. Mumtaz, M. H. Syed, M. A. Hosani, and H. H. Zeineldin, "A simple and accurate approach to solve the power flow for balanced islanded microgrids," in *2015 IEEE 15th International Conference on Environment and Electrical Engineering (EEEIC), Rome, Italy*, 2015, pp. 1852–1856. DOI: 10.1109/EEEIC.2015.7165454.

[9] A. BELAYATI and M. A. BOUDALI, "Load flow analysis for islanded ac microgrid," M.S. thesis, IGEE, 2021.

[10] C. BELAHADJI and H. ZAOUI, "Load flow solution for islanded microgrids using conventional and non-conventional methods," M.S. thesis, IGEE, 2019.

[11] S. Chieng Kai, T. Tay Lea, N. Janardan, and M. Syafrudin, "Load flow analysis using improved newton-raphson method," *Trans Tech Publications, Switzerland*, 2015.

[12] M. Faisal, S. Mazheruddin, A. H. Mohamed, and H. H. Zeineldin, "A novel approach to solve power flow for islanded microgrids using modified newton raphson with droop control of dg," *IEEE Transactions on Sustainable Energy*, Dec. 2015. DOI: 10.1109/TSTE.2015.2502482.

[13] G. C. Kryonidis, E. O. Kontis, A. I. Chrysochos, K. O. Oureilidis, C. S. Demoulias, and G. K. Papagiannis, "Power flow of islanded ac microgrids: Revisited," *IEEE Transactions on Smart Grid*, vol. 9, no. 4, pp. 3903–3905, 2018. DOI: 10.1109/TSG.2018.2799480.

[14] C. Li, S. K. Chaudhary, M. Savaghebi, J. C. Vasquez, and J. M. Guerrero, "Power flow analysis for low-voltage ac and dc microgrids considering droop control and virtual impedance," *IEEE Transactions on Smart Grid*, vol. 8, no. 6, pp. 2754–2764, 2017. DOI: 10.1109/TSG.2016.2537402.

[15] D. Singh, R. K. Misra, and D. Singh, "Effect of load models in distributed generation planning," *IEEE Transactions on Power Systems*, vol. 22, no. 4, pp. 2204–2212, 2007. DOI: 10.1109/TPWRS.2007.907582.

[16] K. Hesaroor and D. Das, "Improved modified newton raphson load flow method for islanded microgrids," in *2020 IEEE 17th India Council International Conference (INDICON), New Delhi , India*, 2020, pp. 1–6. DOI: 10.1109/INDICON49873.2020.9342587.